J. Fluid Mech. (1987), *vol.* 174, *pp.* 233–270
Printed in Great Britain

Large-scale vortex structures in turbulent wakes behind bluff bodies. Part 1. Vortex formation processes

By A. E. PERRY AND T. R. STEINER
Department of Mechanical Engineering, University of Melbourne, Parkville, 3052, Victoria, Australia

(Received 30 July 1985 and in revised form 12 May 1986)

An investigation of turbulent wakes was conducted and phase-averaged velocity vector fields are presented, as well as phase-averaged and global Reynolds normal and shear stresses. The topology of the phase-averaged velocity fields is discussed in terms of critical point theory. Here in Part 1, the vortex formation process in the cavity region of several nominally two-dimensional bluff bodies is investigated and described using phase-averaged streamlines where the measurements were made in a nominal plane of symmetry. It was found that the flows encountered were always three-dimensional and that the mean-flow patterns in the cavity region were quite different from those expected using classical two-dimensional assumptions.

1. Introduction

Over recent years a considerable amount of work has been carried out at the University of Melbourne on the description of eddying motions in wakes and jets. Much of this work has been devoted to flow at moderate Reynolds numbers where in some cases the eddying motions can be made perfectly periodic in time by external stimulation such as an acoustic excitation (e.g. see Perry & Lim 1978; Perry, Lim & Chong 1980; Perry, Chong & Lim 1982; Perry & Tan 1984). Flow-visualization techniques and instantaneous velocity-vector-field measurements applicable to given phases of the vortex-shedding cycle at the source of the wake or jet showed that many flows could be qualitatively characterized by a relatively small number of distinct features located within the flow field.

In much of the work just mentioned, the phenomena studied would be best described as unsteady periodic laminar flows. Some fully turbulent wakes behind bluff bodies have also been examined, where the vortex shedding has been deliberately 'locked in' to an oscillation of the body. Perry & Watmuff (1981) looked at large-scale phase-averaged velocity-vector-field patterns in the turbulent wake of an ellipsoidal body at high Reynolds number, with and without imposed oscillations of the body. Several years prior to this, Cantwell (1976) had obtained phase-averaged velocity vector fields in the turbulent wake behind a circular cylinder in cross-flow. In spite of large-scale 'phase jitter' caused in part by modulation in the frequency of vortex shedding at the source, and the fine-scale motions superimposed on the large-scale motions, it was found that the general topological features present in the phase-averaged motions bear a strong resemblance to those in the forced periodic motions in laminar flow.

Many features present in the latter flow cases can be described with the aid of

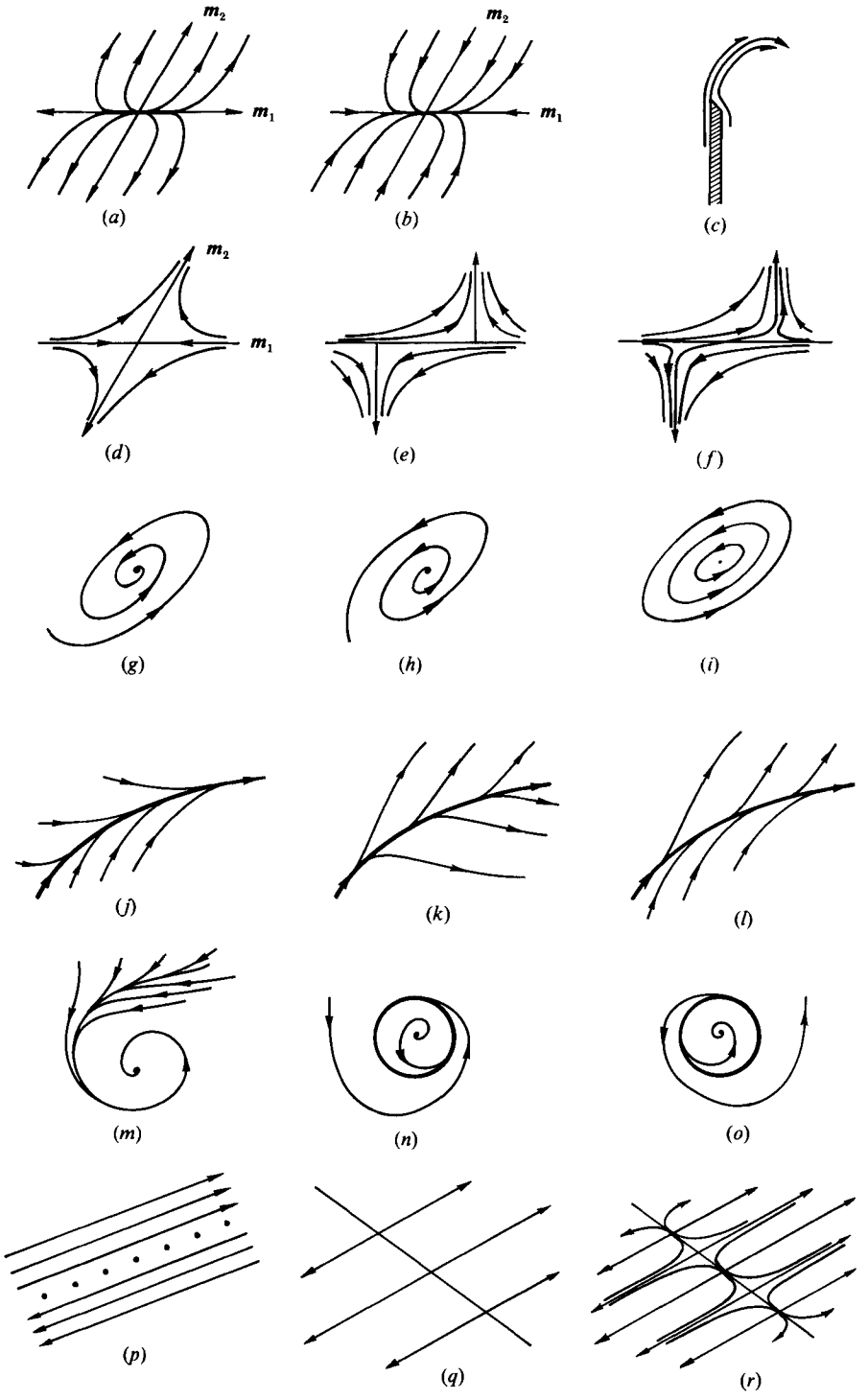

FIGURE 1. For caption see facing page.

'critical-point' theory. Critical-point theory was initially developed by Oswatitsch (1957), Lighthill (1963) and others for the study of 'no-slip' flow in the vicinity of three-dimensional separation points. A critical point is a point in a flow field where the streamline slope is indeterminate. By expressing the velocity field as a series expansion in space about such points, a local solution of the Navier–Stokes and continuity equations can be obtained. This solution may consist of a set of relationships between the various coefficients in the expansion. From this, a classification of all possible regular critical points in a three-dimensional flow field can be derived. Perry & Fairlie (1974) extended the theory to flow away from boundaries and this is highly relevant to eddying motions in free shear-layer flows such as jets and wakes. However, the Perry & Fairlie formulation was incomplete. They truncated their series expansion to include only terms that were first-order in the spatial coordinates, whereas terms up to at least third order must be retained if the complete set of possible critical points is to be obtained. The theory dealing with this more complete set has only recently been formulated by Perry (1984*a*, *b*) and this formulation also includes time dependence.

Shown in figure 1 are a number of flow-pattern features. Included in this 'pictorial dictionary' of features are a selection of critical-point patterns. These patterns consist of streamlines obtained by integrating the components of the three-dimensional velocity field that are resolved onto any plane that contains the critical point. Such patterns will be referred to as 'sectional streamline patterns' and more will be said about these in Part 2 of this paper (Steiner & Perry 1986). Of course, different sectioning planes through the flow surrounding a critical point will give different patterns. Here (Part 1) we confine our investigations to planes of symmetry where the velocity vectors are assumed not to pierce the plane but to lie in it. Thus in this plane we have true streamlines rather than sectional streamlines. Critical-point patterns have been examined and classified by Kaplan (1958) and Minorsky (1947, 1962). Included in this classification are degenerate or 'borderline' cases which exist between different types of critical points. For example, a 'centre' is a borderline case between a stable focus and an unstable focus. The degenerate 'node-saddle' is a borderline case between a node and a saddle (see figure 1).

Another important flow-pattern feature is the bifurcation line which may be either open or closed. A closed bifurcation line will be referred to as a 'limit cycle' in this work. Some of the theoretical properties of bifurcation lines are given in Hornung & Perry (1984), and Perry & Hornung (1984). Examples of these flow features are also included in figure 1.

The features shown in figure 1 have been found to show up quite clearly in the phase-averaged patterns in turbulent flows where there is a dominant frequency of vortex formation and shedding at the source (e.g. a bluff body). Of course, the physical basis for their properties might need modification from that given in earlier

FIGURE 1. 'Pictorial dictionary' of flow features. (*a*) Unstable node†, (*b*) stable node†, (*c*) salient edge, (*d*) saddle†, (*e*) idealized dislocated saddle (unsteady flow only)‡, (*f*) dislocated saddle on a finite thickness shear layer, (*g*) stable focus, (*h*) unstable focus, (*i*) centre, (*j*) negative open bifurcation line (stable), (*k*) positive open bifurcation line (unstable), (*l*) meta-stable open bifurcation line (neutrally stable), (*m*) negative bifurcation line associated with stable focus, (*n*) negative closed bifurcation line (stable 'limit cycle'), (*o*) positive closed bifurcation line (unstable 'limit cycle'), (*p*) simple shear (2-D and degenerate), (*q*) degenerate 'node-saddle' combination, (*r*) non-degenerate combination of nodes and saddles.

† $\boldsymbol{m}_1$ and $\boldsymbol{m}_2$ are eigenvectors and are orthogonal in irrotational flow. ‡ Dislocated saddles may be considered as two half-saddles sitting back-to-back on a vortex sheet.

works, which looked at unsteady laminar flows. Perry & Watmuff (1981) did some preliminary work on the effect of 'phase jitter' on the appearance of critical points. The effect of superimposed fine-scale motions, such as those existing in turbulent flows, is not known. Broadly speaking, the physical interpretations attached to the various features should be similar to those relevant to the unsteady-laminar-flow cases. For example, a focus seen in a plane of symmetry is consistent with a vortex being subjected to an axial straining normal to that plane. As will be seen later, a limit cycle is consistent with the presence of a multi-celled vortex structure. A node in a plane of symmetry requires that there exist saddles in certain planes orthogonal to the plane of symmetry (see Perry *et al.* 1980; Perry 1984*a*).

Critical points and bifurcation lines are the salient features of a flow pattern. The topological classification provides a useful and unambiguous language for describing complex flow fields, In addition, a knowledge of their properties gives clues to the physical processes occurring in the flow. By observing the phase-averaged streamlines in a plane of symmetry of a complex three-dimensional flow pattern, certain out-of-plane features may be deduced using critical-point theory.

Perry *et al.* (1982) used multiple exposures of Prandtl's movie for flow past a circular cylinder made visible with aluminium particles on a free surface, and were able to deduce the essential topological structure of the streamline patterns at each stage of the vortex-shedding cycle. Such flow-visualization techniques cannot be used where the flow is turbulent and some statistical method with anemometry is then needed to obtain phase-averaged vector fields. Perry & Watmuff (1981), and Cantwell & Coles (1983) attempted such measurements using 'flying-hot-wire' techniques. The bias velocity imposed on the wires overcame the directional ambiguity problems of hot-wires placed in regions of reverse flow. However, the results were largely unsatisfactory in the cavity region because of insufficient spatial resolution.

In Part 1 of this paper, the authors make a concerted effort to obtain some satisfactorily detailed phase-averaged velocity vector fields in the cavity region of a nominally two-dimensional bluff plate set normal to the flow, and behind a similar plate set at an angle of attack to the flow. These plates were mounted horizontally across the wind tunnel. In Part 2 (Steiner & Perry 1986), the corresponding far-field wake patterns are determined, and also some far-field wakes behind a variety of three-dimensional bodies are presented.

2. Apparatus and procedures

2.1. *Apparatus*

The University of Melbourne large flying-hot-wire system was used for all the experiments described here. This system has been described by Watmuff, Perry & Chong (1983) but some of the details have since been modified. The system is different from that described by Perry & Tan (1984) which was a miniaturized flying-hot-wire system of different design.

In experiments described by Cantwell (1976), and Cantwell & Coles (1983) hot-wire probes were mounted at the ends of a beam which was rotated about its mid-point. The system used here is shown in figure 2. An air-bearing 'sled' is used to carry a hot-wire probe rectilinearly with a significant bias velocity through highly turbulent flows. This bias velocity allows meaningful measurements to be taken in regions of reverse flow as well as improving the accuracy of measurements taken in regions of high turbulence intensity.

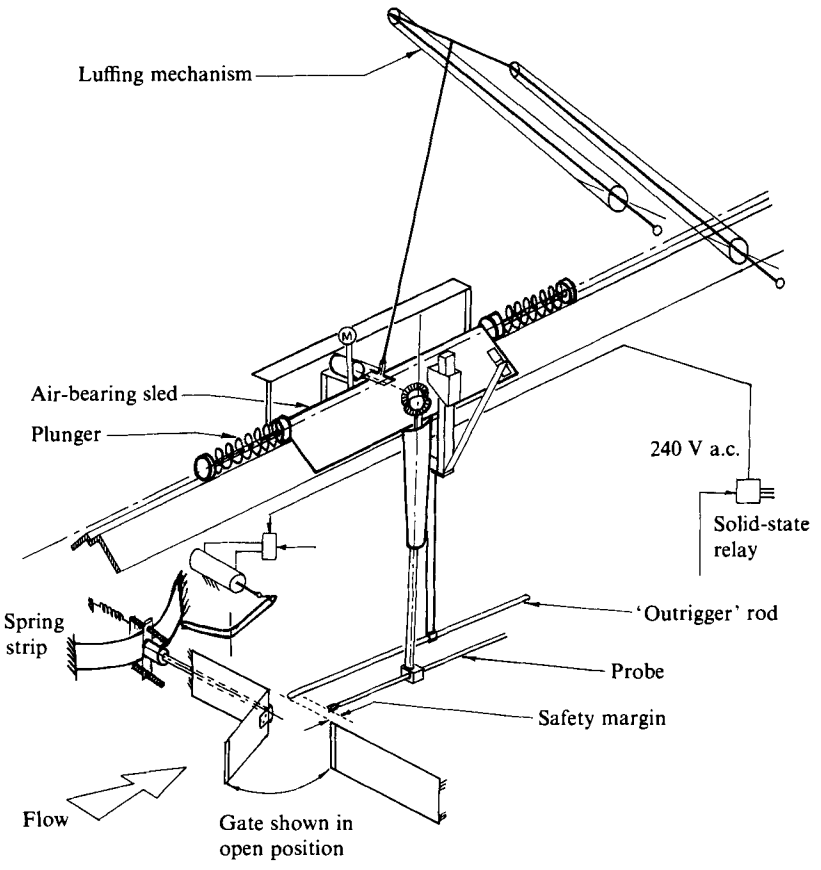

FIGURE 2. Schematic representation of the flying-hot-wire apparatus and mechanism used to open gate in body.

The sled rides on a rail situated above the roof of the wind-tunnel working section. A 'sting' passes through the roof via a slot which is sealed with flaps. The hot-wire probe is supported at the end of the sting. The sled assembly is propelled back and forth by a pneumatic ram, and a special system of springs ensures that the motion is smooth. A straight-line motion mechanism called a 'luffing mechanism' allows air hoses and electrical cables to be attached to the sled without impairing its motion.

Data is sampled during the upstream motion of the sled. In order to obtain meaningful results in the cavity region where there is flow reversal, the wires need to come as close to the body as possible while still moving at high speed. A nominally two-dimensional bluff plate was chosen since it represents the simplest bluff-body case, and has the virtue of fixed separation points. A gate was incorporated in the plate to allow the probe to pass through without damage. This gate was quickly opened at the last moment permitting valid samples to be taken to within 1 cm of the plate.

The apparatus for opening the gate is shown in figure 3. This mechanism applied a small closing force to the gate. An 'outrigger' rod which rode on the sled needed only to tap the gate with a very small force to cause the mechanism to release. This rod was supported at the end of a sting entirely separate from the one which supported the probe so as to minimize the vibrations being transmitted to the probe.

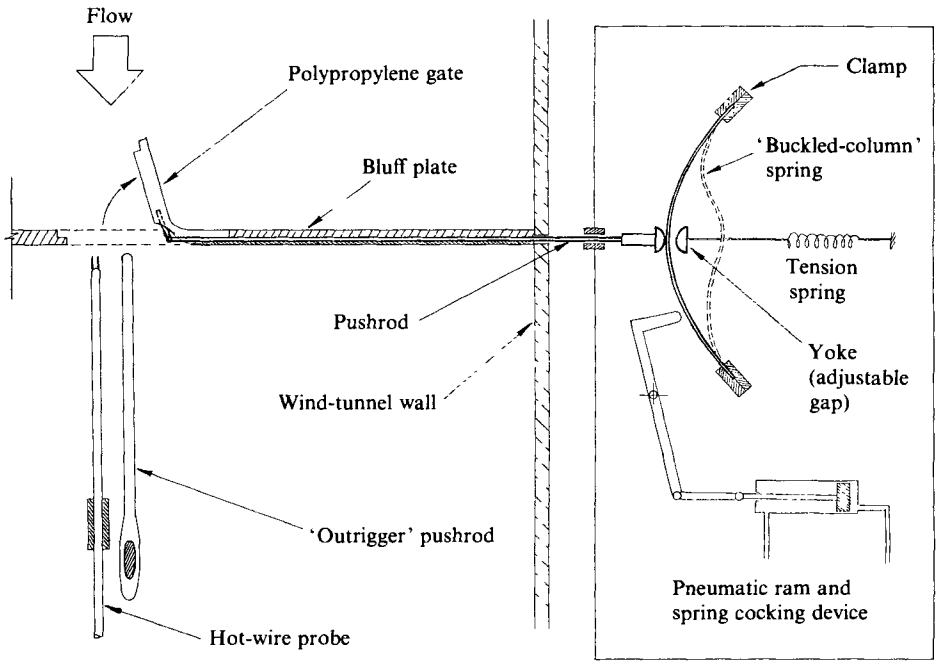

FIGURE 3. Schematic diagram showing mechanism used to open gate in bluff body.

The rod was sufficiently far from the probe to have negligible effect on velocity measurements. On release, the mechanism rapidly opened the gate allowing the probe to pass through at high speed. No data was accepted once the gate opened. A distance of about 300 mm was required to bring the sled to rest before its motion was reversed. On the return stroke of the sled the gate mechanism was re-cocked once the probe was safely clear.

The disturbance of the flow caused by the opening of the gate and the motion of the stings in the working section was convected downstream and it was estimated that there existed at least 1.25 m of uncontaminated flow immediately behind the body by the time the sled began its forward pass. As the region of interest for the near-wake cases was confined to the 0.5 m or so nearest to the body, flow contamination was considered not to be a problem.

2.2. *Data acquisition*

Unlinearized constant-temperature hot-wire anemometers were used throughout, and these were constructed and used according to the guidelines of Perry (1982). The cross-wires were 'matched' and dynamically calibrated. Calibration equations giving the velocity components as functions of the two anemometer voltages were established, and these took into account the nonlinearities of hot-wire anemometers.

All data-acquisition and 'phase-sorting' techniques were essentially the same as outlined by Perry & Watmuff (1981) and Watmuff *et al.* (1983). They used an electronic simulation to check the correct functioning of the rather complicated data acquisition and sorting. A much more direct method was devised to check these techniques for this work. The rotating 'barbers' pole' shown in figure 4 forms the basis of this check. An optical scanning head containing LEDs and a photodetector is carried on the end of the sting and simulates the hot-wire probe, while the light

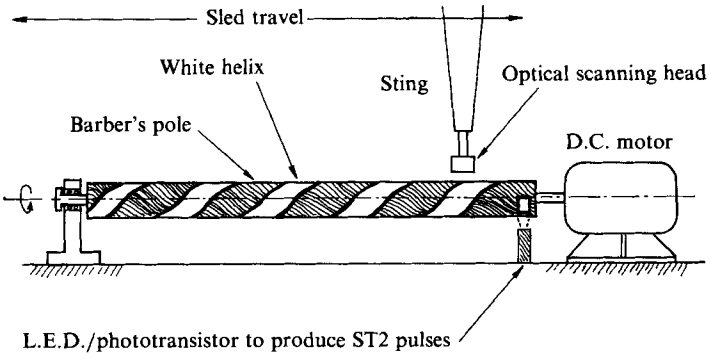

FIGURE 4. Schematic diagram of 'barber's pole' used for testing data acquisition and sorting methods.

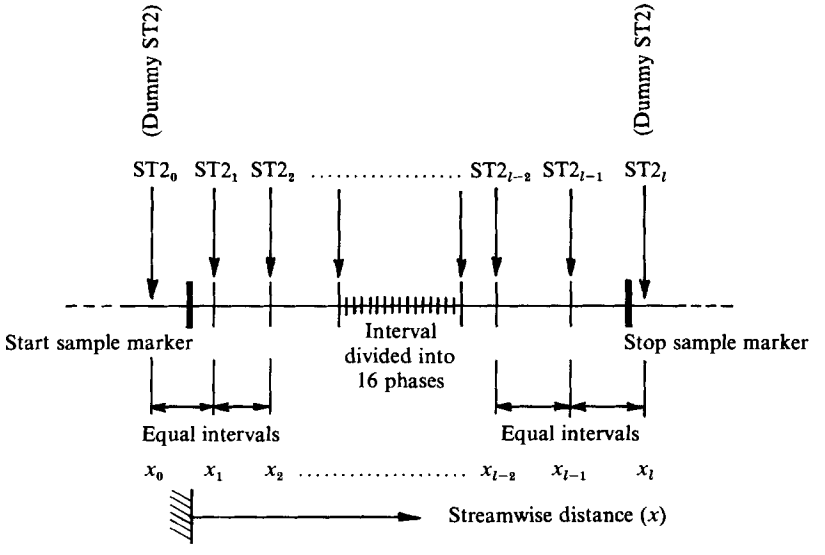

FIGURE 5. Allocation of samples into phases. Here x is streamwise distance upstream. In the remainder of the paper it is distance downstream.

and dark bands on the rotating pole simulate eddies moving down the working section. Data is sampled and sorted on the basis of the phase of rotation of the pole using the same software as used for experiments. It was possible to simulate accelerating eddies by having helical bands of varying pitch on the barbers' pole. This demonstrates a major advantage of traversing the probe in a streamwise direction through many stations. Velocity vector fields may be produced independent of any Taylor hypothesis assumption, and this is vital if the flow is to be correctly interpreted in regions of rapid flow development.

Data was sampled every cm in the streamwise direction, and the velocity of the sled was known at all times by frequency demodulation of streamwise position pulses spaced 1 mm apart.

Phase detection was carried out using a stationary normal hot-wire probe situated near to but just outside of the near-wake region in the non-turbulent part of the flow. It was typically about 150 mm from the plane of symmetry and its optimum position in the other coordinates was found by trial and error.

For the results presented here, a power-spectral-density graph of the phase-detector signal showed a very strong dominant peak. The signal was band-pass filtered with a width of about one decade, the centre frequency being adjusted to correspond with the spectral peak. This gave a near-sinusoidal signal which modulated slightly in period and in amplitude. This signal was then passed through a Schmitt trigger and each leading edge of the resulting pulse train (referred to as ST2 pulses) was used to define the beginning of a new vortex-shedding cycle.

Figure 5 shows how these ST2 pulses are distributed in one pass of the sled as it moves upstream. Since the velocity of the sled was approximately constant during the entire pass, its position was proportional to time and so sixteen spatial intervals between two successive ST2 pulses correspond to sixteen phase intervals of the vortex-shedding cycle. Unfortunately, at the end of the data-sampling length when the probe reaches the body, the phase detection is upset by the opening of the gate and another ST2 pulse is needed after this event in order to allocate data taken in the cavity region to the correct phase intervals. This was done by creating a 'dummy' ST2 pulse (labelled $ST2_l$ in figure 5) which assumed that the period of the last sampled vortex-shedding cycle was the same as the preceding period. For technical reasons a dummy $ST2_0$ pulse was also created at the downstream end of the sampling length. The period between ST2 pulses was estimated to have had a standard deviation of 12 % of the mean value.

2.3. *Convergence of data*

Randomness in vortex shedding causes considerable difficulties in obtaining phase-averaged vector fields. In the deterministic experiments of Perry & Tan (1984), an entire vector field in a plane of symmetry could be obtained in about 7 min.

Here in this non-deterministic flow, attempts to obtain adequate data convergence solely by accumulating a large sample population would have required extremely long running times. Hot-wire drift over such long running times would have caused major difficulties. To obtain acceptable convergence within reasonable running times the following techniques were used.

The hot-wire signals were low-pass filtered at about one decade above the vortex-shedding frequency, and the data was 3-point smoothed in the streamwise direction with appropriate weighting given by the sample population at each point for each phase. This smoothing was carried out over a lengthscale smaller than the spatial limit imposed by phase resolution. Three-point smoothing was then carried out in both the streamwise and cross-stream directions. With these techniques it was found that 800 samples per position (or about 50 per position per phase) were sufficient for reasonable data convergence. This required a running time of about 40 min per horizontal row. Data acquisition time was typically 8 h for each case and the longest case required about 16 h. Time required for calibrations and for running maintenance to the mechanical hardware was usually equivalent to the data acquisition time. Without filtering and smoothing however, our apparatus would need nearly 13 days of data acquisition time to obtain the same sample population as achieved by Cantwell & Coles. Their apparatus scanned the flow more rapidly by swinging hot wires through a circular arc at the end of a whirling arm and so they only took 27 h to gather 40 times the sample population here. Although the apparatus used here was much slower, it had the advantage of being able to scan a much larger region of the flow, and was better suited for exploring the cavity region. A further benefit was gained as a result of data reduction being virtually complete at the end of the experiment. An investigation of the effect of data convergence on

Case	Experiment	Reynolds number and relevant lengthscale (l)	A	$St = \frac{fl}{U_\infty}$	Blockage ratio	U_∞ m/s
1	Near wake 2-D normal body (no end plates fitted)	20000 – Projected height (0.10 m)	9.4	0.170	0.246	2.971
2	Near wake 2-D inclined body (no end plates fitted)	14100 – Projected height (0.071 m)	13.2	0.161	0.174	2.954
3	Near wake 2-D normal body (end plates parallel)	18900 – Projected height (0.10 m)	5	0.215	0.246	2.814
4	Near wake 2-D normal body (end plates divergent)	21900 – Projected height (0.10 m)	5	0.248	0.246	3.253

TABLE 1. Some experimental parameters. St = Strouhal number where f is the frequency in Hz of vortex shedding; U_∞ is the free-stream velocity measured about 1 m upstream of the bodies; A = aspect ratio.

the appearance of phase-averaged velocity field patterns is discussed in the Appendix.

The problems of hot-wire drift encountered by Perry & Watmuff (1981) were approached as follows. Calibrations were performed before and after runs, and if the calibration constants changed by less than 2 % then all data were corrected assuming a linear drift in time. If the calibration constants varied by more than 2 % the data would be rejected. Running checks were used to detect any significant drift.

2.4. *Reflection of data*

Properties of antisymmetry in vortex shedding were assumed in order to help keep running times down. This also helped to overcome the physical limitation of the probe traverse which prevented the probe from being carried at a height much above the plate centreline. In the cases where the plate was set normal to the free-stream flow, data were collected along horizontal rows at and below the centreline. It was assumed that the vortex formation above the plate centreline was 180° out of phase relative to that below. Thus by reflecting appropriate data about the plate centreline one could obtain the complete velocity field for a given phase.

In the case of the inclined plate, the assumption of antisymmetry is not valid and the complete vector field was obtained in two runs. The plate and the phase detector were inverted between these two runs.

2.5. *Computation of streamlines*

Velocity vectors were assembled at points that formed a grid of square elements each 1 cm × 1 cm. All the streamlines presented here were calculated by integrating this velocity data. This was achieved by using a two-dimensional cubic spline interpolation between the grid points, coupled with a modified second-order predictor–corrector integration technique. In this way it was possible to eliminate the uncertainties inherent when sketching in streamlines by hand. Spline interpolation does not impose any further smoothing on the velocity field.

3. Results

This work produced a large amount of data which could not be presented here owing to space limitations. The full details and results from experiments performed

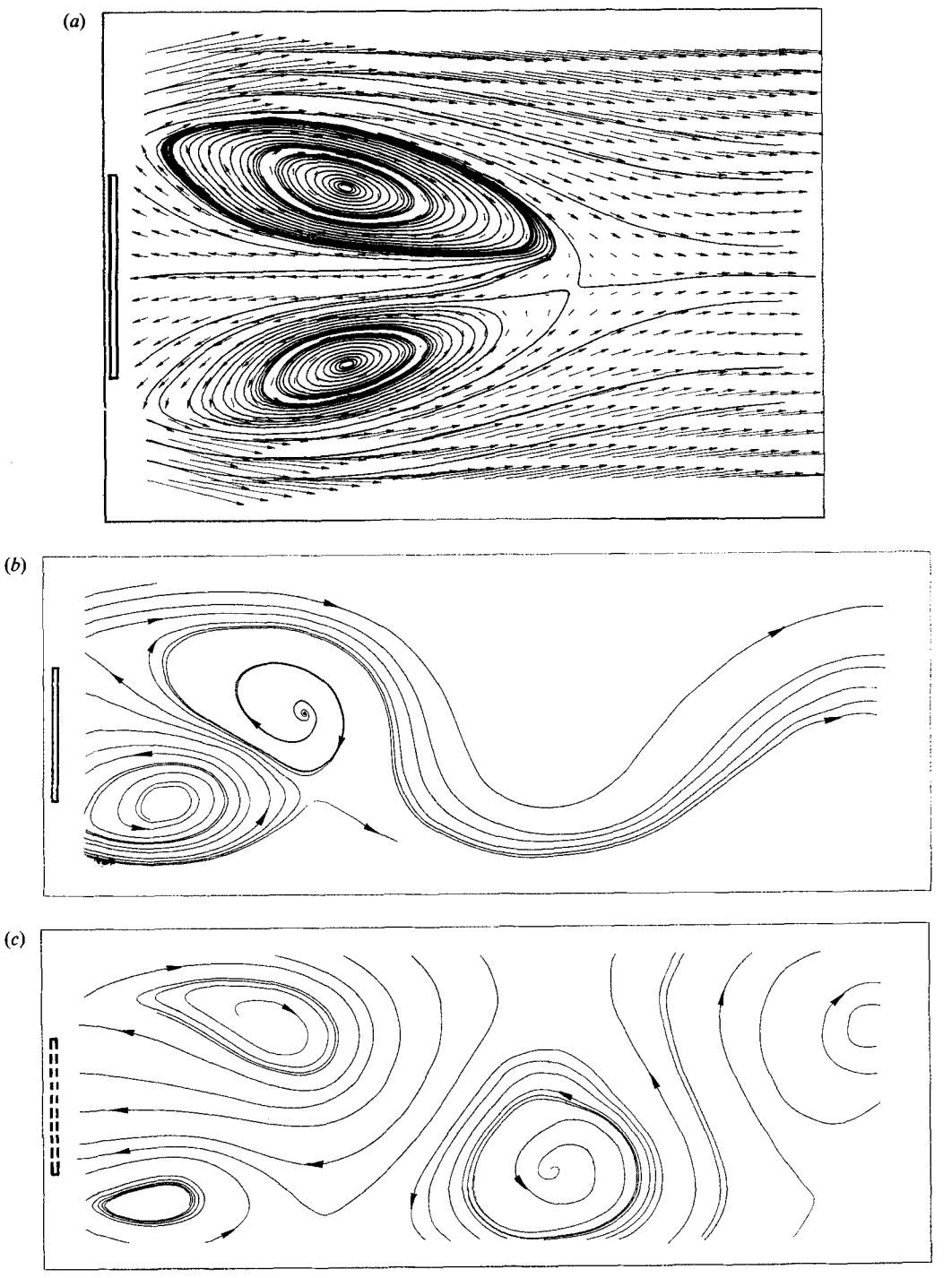

FIGURE 6. (*a*) Mean velocity vector field and integrated streamline pattern for case of nominally two-dimensional body with no end plates. (*b*) Integrated streamline pattern for flow in the wake of the normal bluff body with no end plates attached, at phase one of the vortex-shedding cycle. Observer stationary relative to the bluff body. (*c*) Same as (*b*), except that the observer is moving downstream at 2 m/s. The body is indicated by 'phantom' lines since it is not stationary in the observers frame of reference.

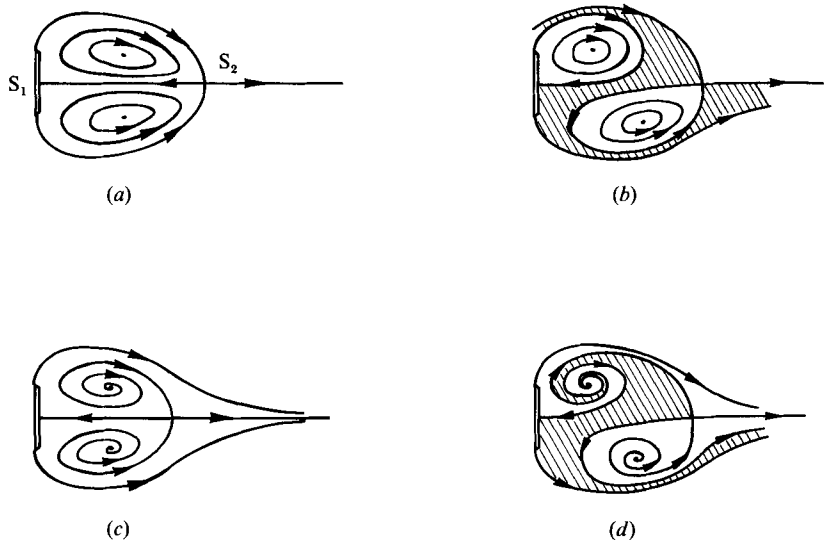

FIGURE 7. Some simple mean flow patterns in the wakes of nominally two-dimensional bluff bodies: (*a*) two-dimensional and symmetrical; (*b*) two-dimensional and asymmetrical; (*c*) three-dimensional and symmetrical; (*d*) three-dimensional and asymmetrical.

may be found in Steiner (1984). Table 1 lists some experimental parameters for the cases presented.

3.1. *Near wake for a normal bluff body*

Figure 6(*a*) shows the time-mean flow pattern in the cavity region behind a normal bluff body with no end plates attached. This pattern was obtained by ensemble averaging all the phase-averaged data. Figure 6(*b*) shows the integrated phase-averaged streamline pattern for phase 1 of this case. Eddying motions are clearly seen only in the near wake and not further downstream where the pattern shows up as wavy streamlines. An observer moving downstream with the convection velocity of the far-wake eddies sees a different pattern (see figure 6*c*) in which the far-wake eddies are now clearly seen, but the near-wake eddies appear distorted. Figure 7(*a*) shows the mean flow pattern expected using conventional assumptions of perfect two-dimensionality and symmetry. In such a pattern only saddles and degenerate centres are possible. The saddle points S1 and S2 may be joined giving a 'closed' cavity as a consequence of the assumption of symmetry.

Two patterns are said to be topologically equivalent if they can be forced to correspond by appropriate distortion, as if the patterns were drawn on sheets which could be deformed at will without tearing. The idealized pattern shown in figure 7(*a*) is said to be topologically unstable since an infinitesimal change in the flow parameters would cause a major change in the topology of such a pattern. Such patterns are unlikely ever to occur in practice since flows that are precisely two-dimensional and precisely symmetrical are extremely rare if not impossible. The measured pattern in figure 6(*a*) is neither symmetrical nor two-dimensional even though it has been measured in a nominal plane of symmetry. The pattern consists of saddles, foci and limit cycles. The asymmetrical appearance of the pattern is due to the existence of a small but finite vertical component of velocity along the centreline of the pattern. This allows integrated streamlines to cross over from the

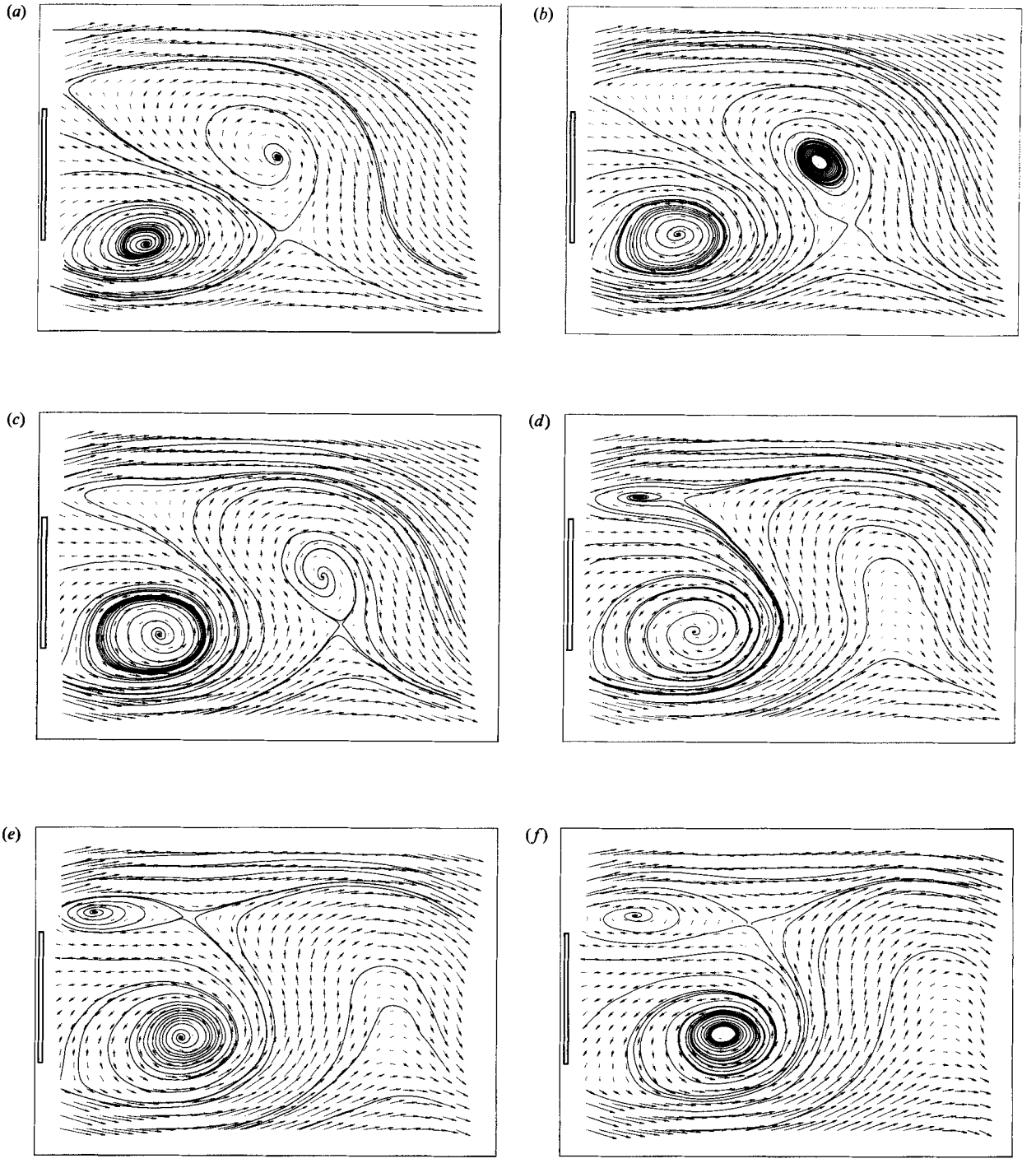

FIGURE 8(*a–f*). For caption see facing page.

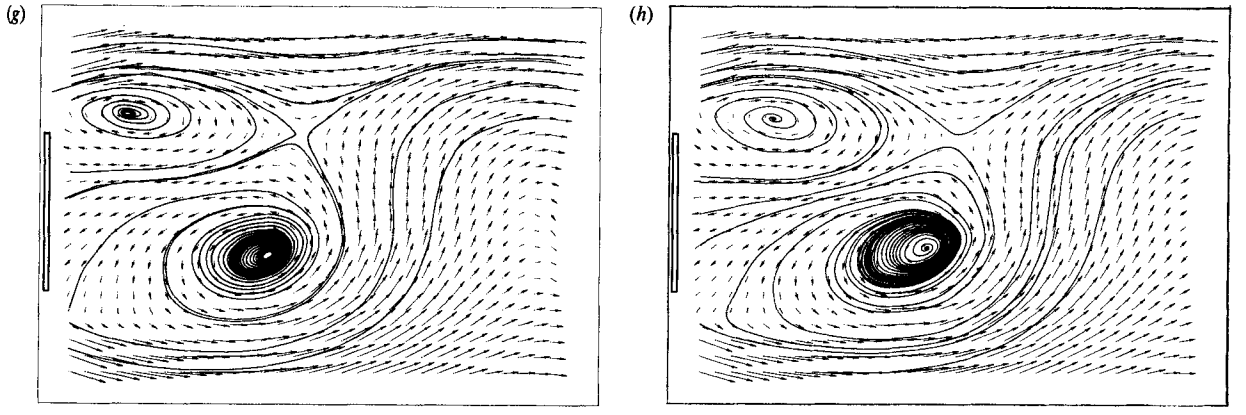

FIGURE 8. Velocity field and integrated streamline pattern for the case of a nominally two-dimensional bluff body with no end plates attached: (*a*)–(*h*) correspond respectively to phases 1–8.

upper half of the pattern to the lower half. As stated above, there is no reason to believe that the flow is precisely symmetrical even though reflection of the data embodies this assumption. Any slight departure from perfect antisymmetry in the vertical component of velocity about the plate centreline will have only a small effect on the pattern, but will have a great effect on how the separatrices are joined (i.e. the streamlines which emanate from saddle points or salient edges). Data along the centreline have a strong influence on this. Hence, the authors contend that for small departures from antisymmetry in the vertical component of velocity, it is justified to retain data along the plate centreline and reflect all data to one side of it. This is preferable to artificially forcing the data along the plate centreline to have a zero component of vertical velocity.

Figures 7 (*b–d*) show some further simple topologies for different cavity flows seen in planes of symmetry. Case (*b*) is an unsymmetrical two-dimensional cavity and an 'alleyway' (shown shaded) penetrates right through the cavity. Flow case (*c*) is three-dimensional and symmetrical and it can be seen that the pattern has a net divergence in the plane of symmetry. This is due to fluid in the mean approaching the plane of symmetry from either side. That is, in this example the vortices are being compressed axially normal to the plane of symmetry. Figure 7 (*d*) shows the pattern in a three-dimensional and unsymmetrical flow. It will be noted that the pattern in figure 7 (*d*) appears to have a similar topology to the mean flow pattern in figure 6, except for the appearance in the experimental data of two nested limit cycles associated with each focus.

Figure 8 shows the phase-averaged plots for the first eight phases of the cycle. The remaining eight phases may be found simply by reflecting these patterns about the centreline. Figure 9 shows the interpretations of the plots given in figure 8. These were obtained using the integrated streamline patterns as a guide, and then sketching in the separatrices. A few additional streamlines have been included to make clear the essence of the topology. Dislocated saddles as mentioned by Perry & Watmuff (1981) are shown only where they are obvious in the integrated streamline plots.

From the sequence of interpretations in figure 9, there is a major difference in the vortex formation process from that described by Perry *et al.* (1982). In figure 9 (*d*) we define what is meant by the terms 'attached' eddy, 'detached' eddy, and 'shed'

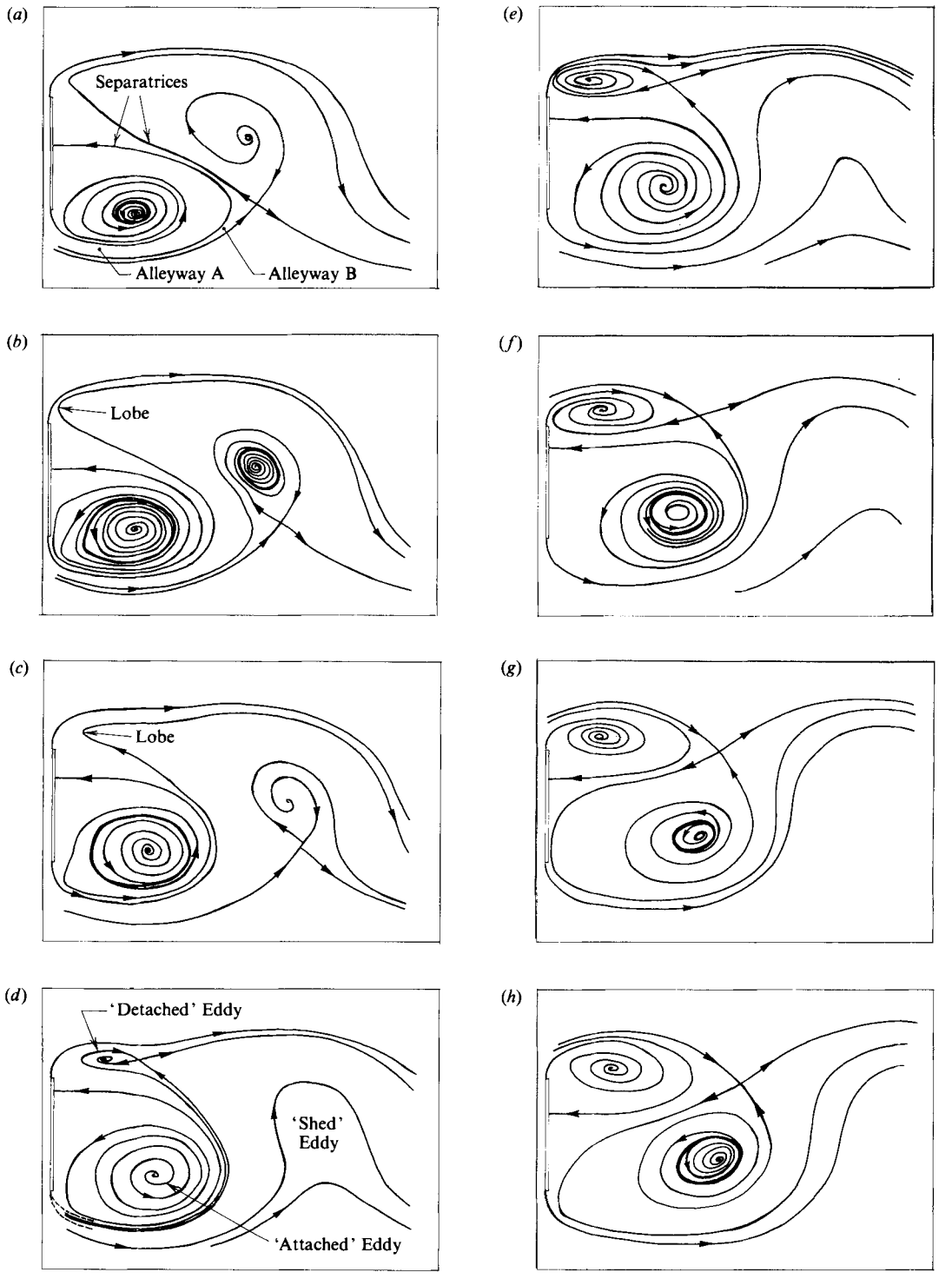

FIGURE 9. Interpretations of integrated streamline patterns given in figure 8. (*a*)–(*g*) correspond respectively to phases 1–8. ----, possible separation streamline positions.

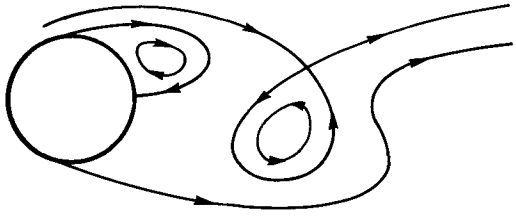

FIGURE 10. Typical instantaneous streamline pattern for the flow in the cavity region behind a nominally two-dimensional cylinder in cross-flow (conjectured by Perry *et al.* (1982)).

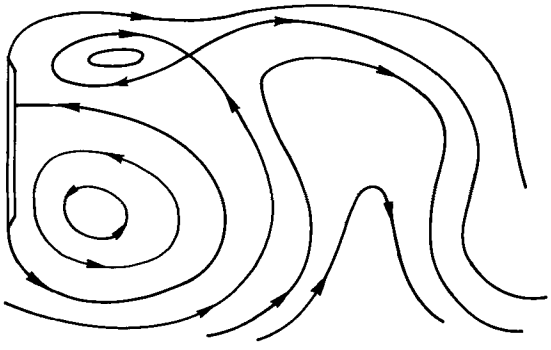

FIGURE 11. Streamline pattern which is a two-dimensional analogue of that for phase 5 in figure 10(*e*).

eddy. An attached eddy has a separatrix that is attached to the plate. Figure 10 shows the typical instantaneous streamline pattern conjectured by Perry *et al.* (1982) for the cavity region behind a nominally two-dimensional circular cylinder in cross-flow with laminar flow. The eddy which is just beginning to form is attached to the cylinder, whereas in figure 9, phases 3–6, it is shown clearly that such an eddy may be detached from the body at formation and become attached at some later stage of the cycle. During the cycle, the appearance of eddies can change from being stable foci to unstable foci. This bifurcation process appears to be consistently accompanied by the appearance of a limit cycle.

Figure 11 is a two-dimensional analogue of phase 5 in figure 9. It can be seen that both figures show an 'instantaneous alleyway' of fluid which penetrates through the cavity. This may be related to the process of entrainment of irrotational fluid into the wake, and also how fluid (such as smoke or dye) can be transported across the wake.

Figure 12 shows a velocity field superimposed on the corresponding boundary of 0.5 phase-averaged intermittency factor. The intermittency was found using the same technique as Cantwell & Coles (1983). When the observer moves with the convection velocity of the pattern, saddles appear to sit on this contour and align themselves with it. This is similar to the result that Cantwell (1976) obtained. This contour gives a rough idea of the shape of a smoke or dye interface and, as shown by Perry *et al.* (1980), the indentations of the interface correspond with alleyways of irrotational fluid penetrating the wake.

Figure 13 shows phase-averaged contours of vorticity, and Reynolds normal and shear stresses. Superimposed on these plots is the contour of 0.5 intermittency factor.

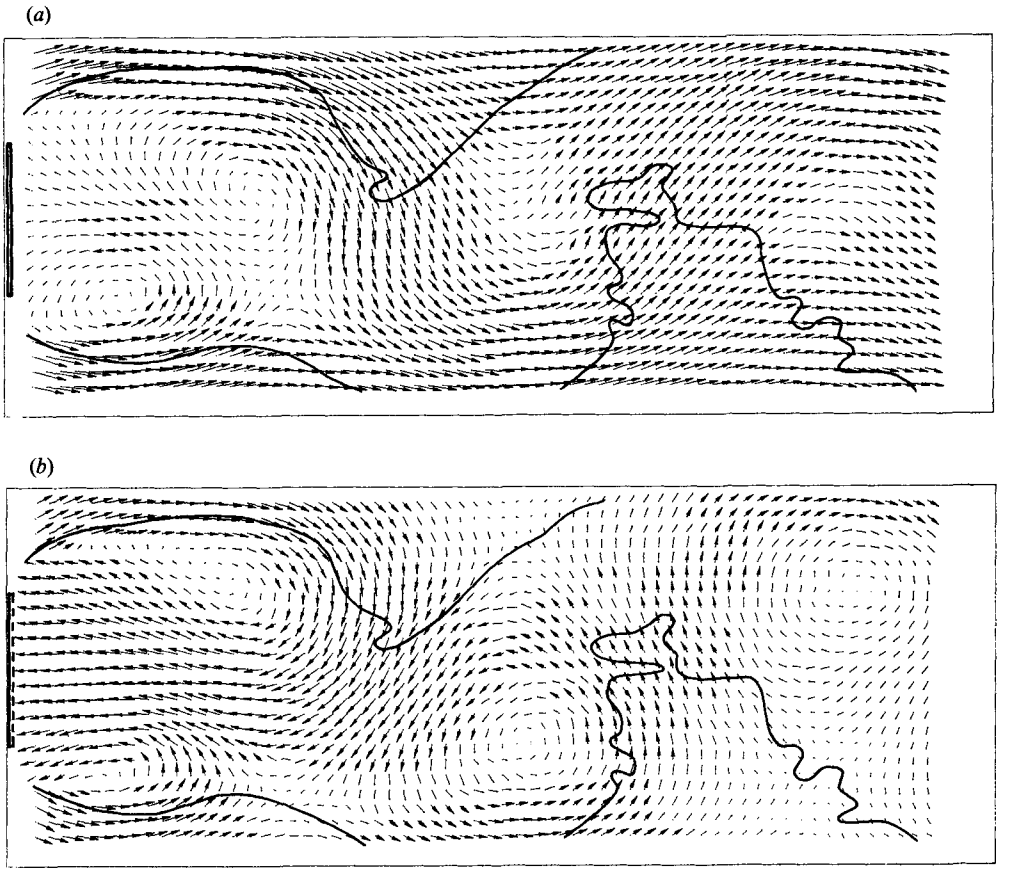

FIGURE 12. (a) Velocity field with boundary of 0.5 intermittency factor superimposed. Observer stationary with respect to the body. (b) As for (a), except that the observer is moving downstream with the far-wake pattern at 2 m/s.

The general features are the same as found by Cantwell & Coles (1983) for flow behind a circular cylinder at a Reynolds number of 140000.

By ensemble averaging the phase-averaged stresses we obtain the mean of the phase-averaged contributions. These are somewhat lower than the global (or total) stresses at the same positions. We are using the same triple decomposition scheme as Cantwell & Coles (1983). The phase-averaged contribution to $\overline{u'^2}$ is about 25% in the near wake. Overbars are used here to denote temporal means. The corresponding proportion for $\overline{v'^2}$ is 40%–50%, and for $\overline{u'v'}$ about 50% which rapidly diminishes to 20% at about three plate heights downstream. Here u' and v' are the perturbations in u and v from their temporal mean values.

Mean velocity and Reynolds-stress profiles, and an explanation of how they were obtained is given in Part 2 of this paper.

Roshko (1954) showed how an estimate of the total circulation of each sign, shed by a bluff body during a single vortex-shedding cycle, could be determined. Davies (1976) used an expression derived from this which gave the fraction of this total circulation that existed in a particular eddy,

$$\alpha = \frac{2St\,\Gamma^*}{(1-C_{\mathrm{pb}})}, \tag{1}$$

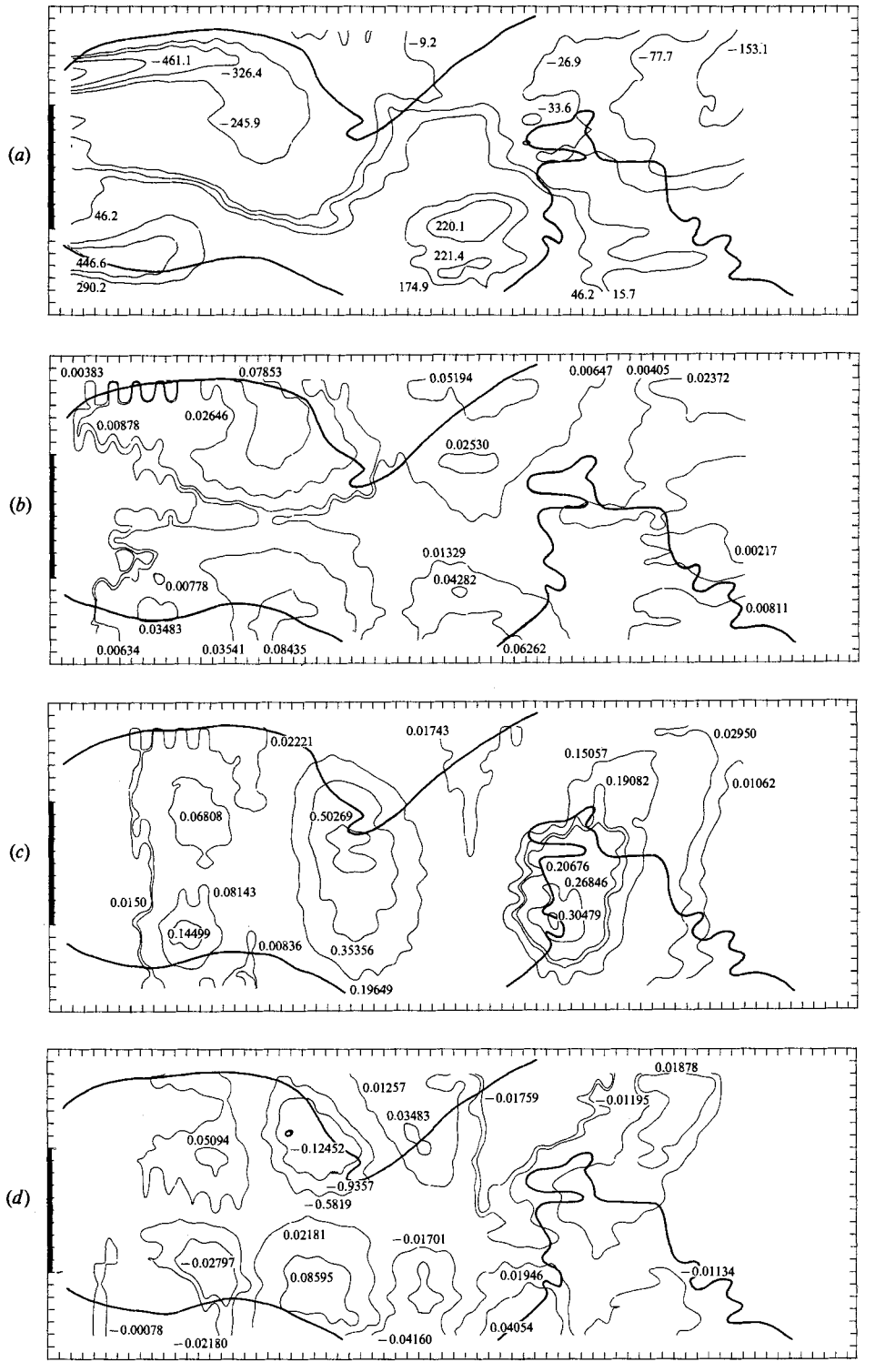

FIGURE 13. Contour plots (*a*) non-dimensionalized phase-averaged vorticity ($\omega d/U_\infty$); (*b*) non-dimensionalized phase-averaged normal stress ($\overline{u'^2}/U_\infty^2$); (*c*) non-dimensionalized phase-averaged normal stress ($\overline{v'^2}/U_\infty^2$); (*d*) non-dimensionalized phase-averaged shear stress ($\overline{u'v'}/U_\infty^2$).

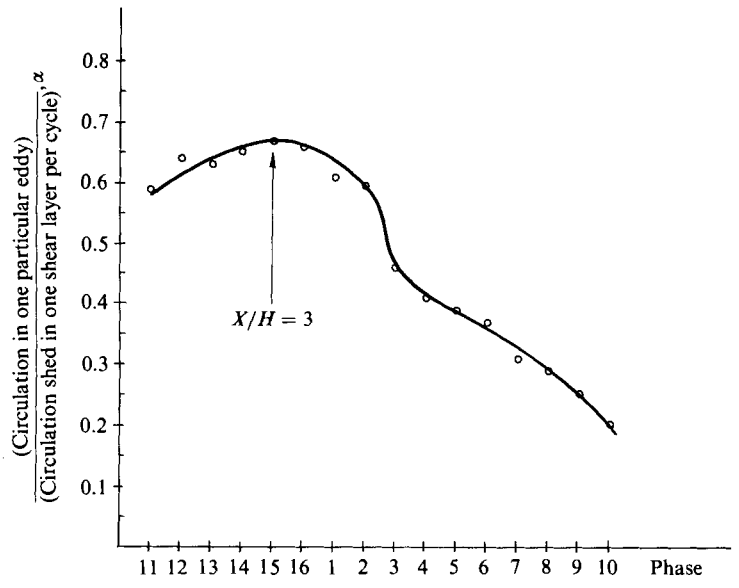

FIGURE 14. Calculated fractional circulation content of an eddy in the wake of the nominally two-dimensional bluff plate with no end plates attached, as a function of phase of the vortex-shedding cycle. The peak value is indicated when the centre of the eddy lies around $X/H = 3$. $\alpha = 2St\Gamma^*/(1-C_{pb})$; $\Gamma^* = \iint (\omega d/U_\infty)\,\mathrm{d}A/\iint \mathrm{d}A$.

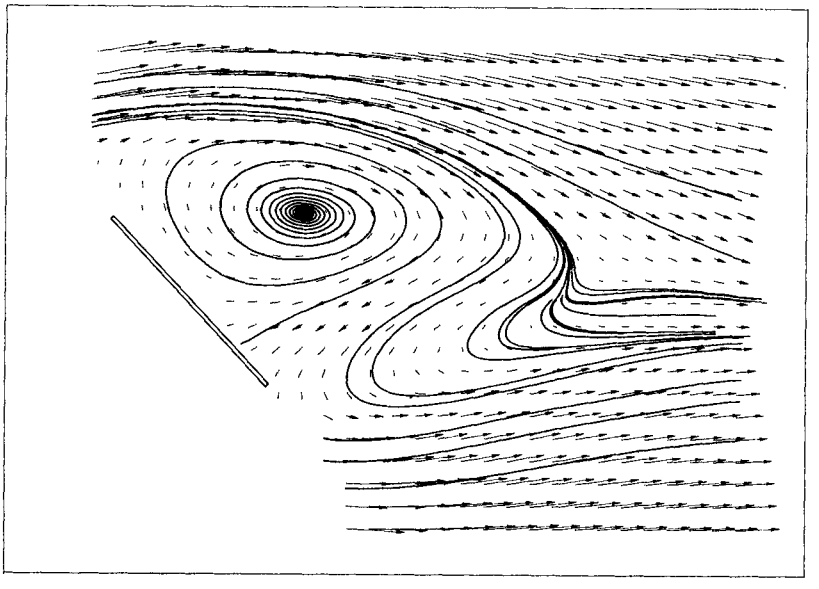

FIGURE 15. Mean velocity vector field and integrated streamline pattern for the case of a nominally two-dimensional body at an angle of attack of 45°.

where α is the fractional circulation remaining in a particular eddy, St is the Strouhal number ($St = fl/U_\infty$, where f = frequency in Hz, U_∞ = free-stream velocity, l = lengthscale of the body), C_{pb} is the base pressure coefficient, Γ is the non-dimensionalized circulation content of the eddy = $\Gamma/U_\infty l$.

The circulation content of an eddy was estimated by summing the phase-averaged

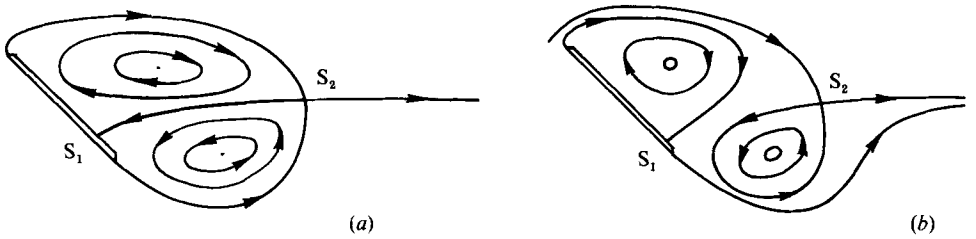

FIGURE 16. Expected mean streamline patterns behind a two-dimensional bluff plate at an angle of attack. (*b*) shows the more likely pattern with saddle points S_1 and S_2 not joined.

vorticity of one sign over an area surrounding the centre of an individual eddy. This was repeated, following the same eddy downstream over different phases of the vortex-shedding cycle, to obtain the graph given in figure 14. The values indicated are of similar order to values given by Davies (1976), Cantwell & Coles (1983) and Nielsen (1970) for a variety of bluff-body flows. The rapid decay of circulation is probably due in part to turbulent diffusion and vorticity cancellation. Also the decay could be due to a continuous convective transfer of vorticity from one vortex of one sign to a vortex of the opposite sign by the interconnecting saddle patterns as mentioned by Cantwell & Coles (1983).

3.2. *Near wake behind an inclined bluff plate*

This case was chosen since it resembles the flow over a nominally two-dimensional stalled wing. Figure 15 shows the mean flow obtained by ensemble averaging all the phase-averaged patterns. Figures 16(*a*, *b*) show patterns that one might expect using conventional two-dimensional thinking. Figure 16(*b*) is more likely since the saddle points are not joined. It is quite obvious that the measured pattern bears little resemblance to either of these conjectured patterns.

Unlike the normal-bluff-plate cases, this case does not have antisymmetric vortex formation and shedding and so it is necessary to show all 16 unique phases. Integrated streamline patterns are shown in figure 17, and their interpretations in figure 18. Although it is clear that vortices are being shed from both sides, only one vortex shows up in the temporal mean plot in figure 15. Again the flow is three-dimensional as evidenced by the existence of foci and limit cycles. The rather unexpected appearance of the pattern in figure 15 is because the vortex formed near the leading edge resides for a longer period in the cavity region than does the trailing-edge vortex. This case shows very clearly a half-saddle residing on a shear layer (see figures 17 and 18, phases 12 and 13).

3.3. *Near wakes behind normal bluff bodies with end plates attached*

In the cases shown so far, the ends of the bluff bodies were simply butted up against the wind-tunnel walls – no particular attention was paid to the end conditions of the bodies. In view of the obvious three-dimensionality of the flow indicated by the preceding results it was decided that end plates would be used in order to reduce this three-dimensionality. The design of the end plates was similar to that of Graham (1969) who also suggested that a small but finite angle between the two end plates could have a beneficial effect. The end-plate design is shown in figure 19. Careful testing indicated that the lowest degree of three-dimensionality was actually obtained when no end plates were used. This was felt to be a consequence of the

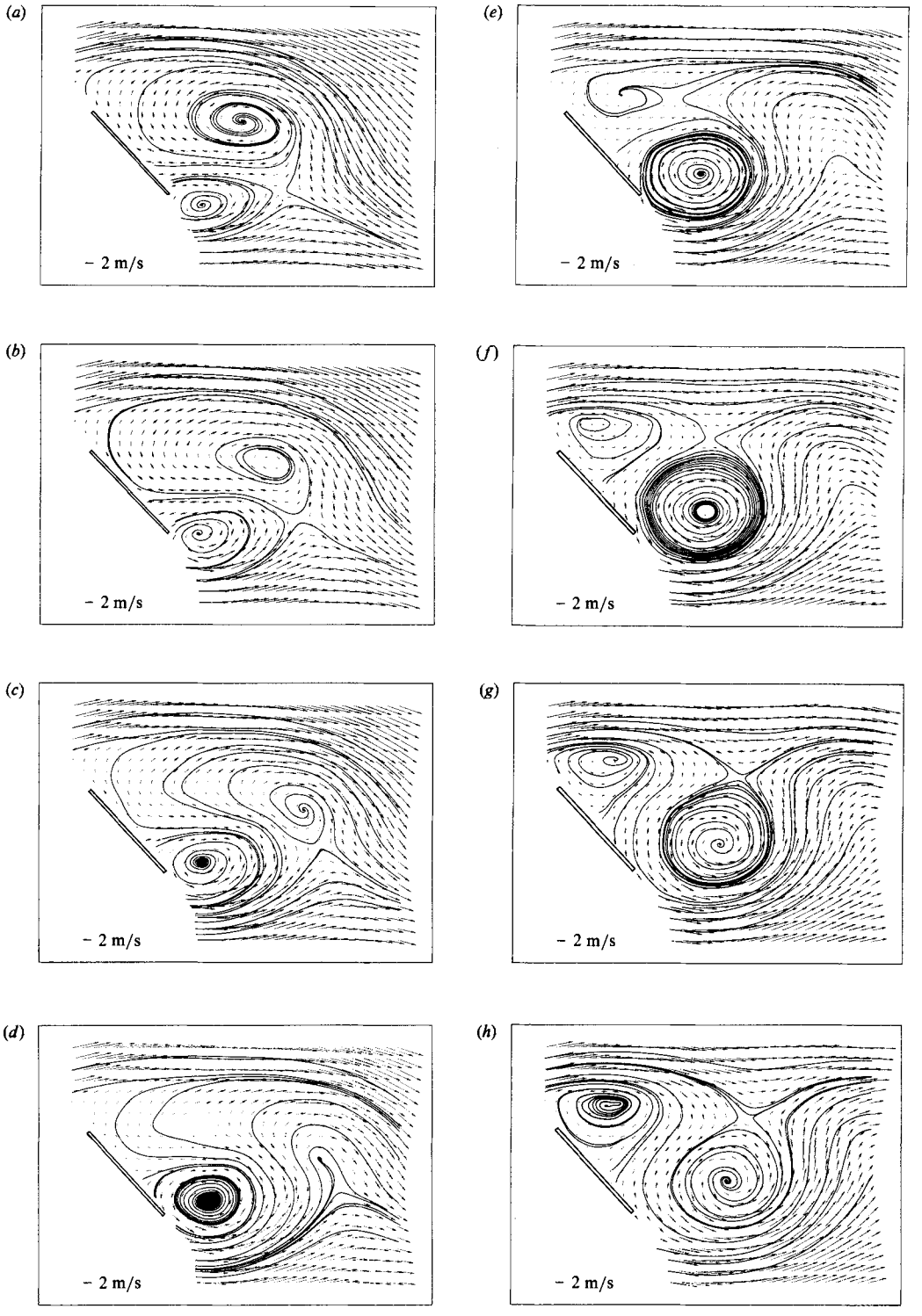

FIGURE 17 (*a–h*). For caption see facing page.

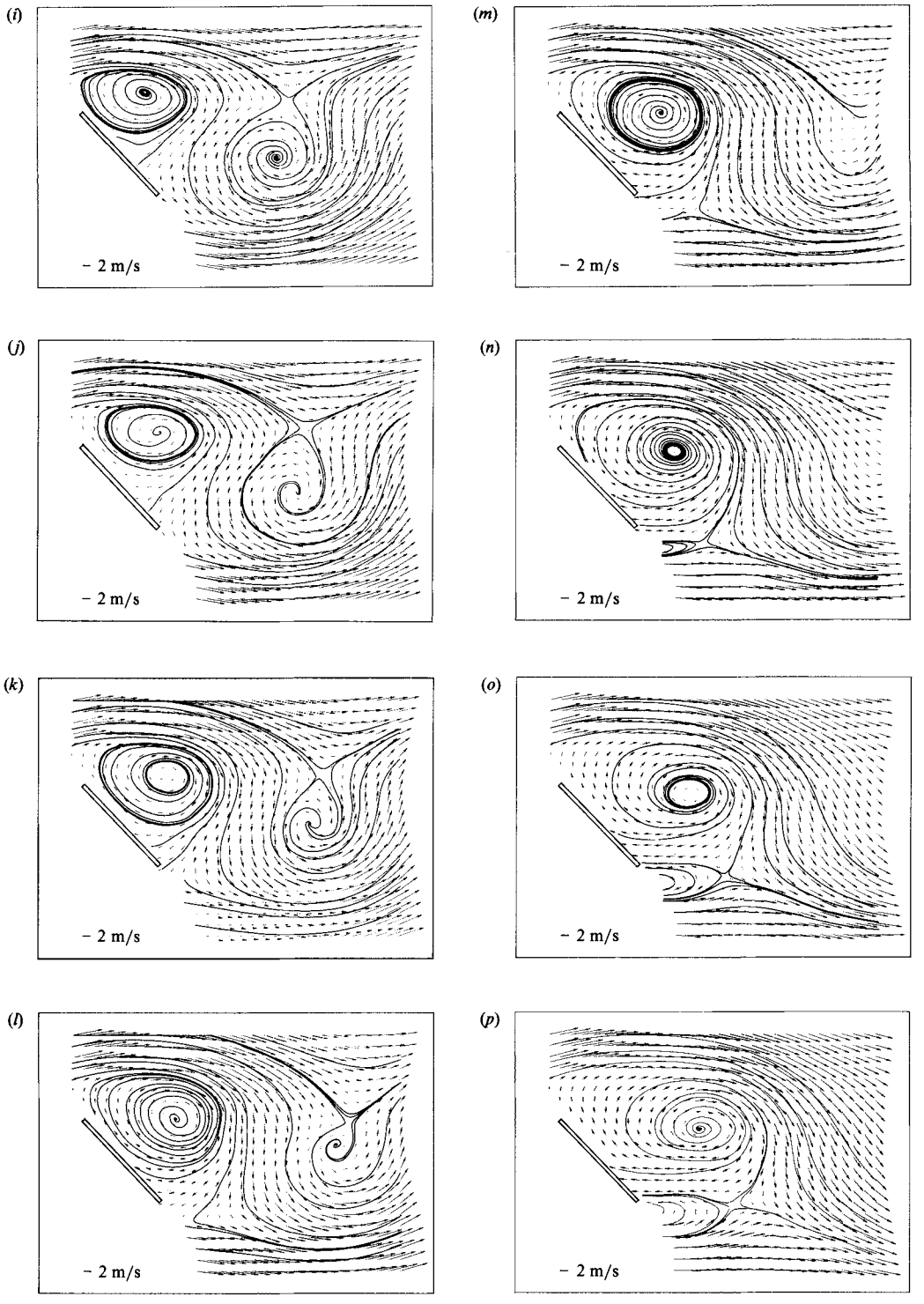

FIGURE 17. Velocity vector fields and integrated streamline patterns behind inclined bluff plate. (*a*)–(*p*) Correspond respectively to phases 1–16.

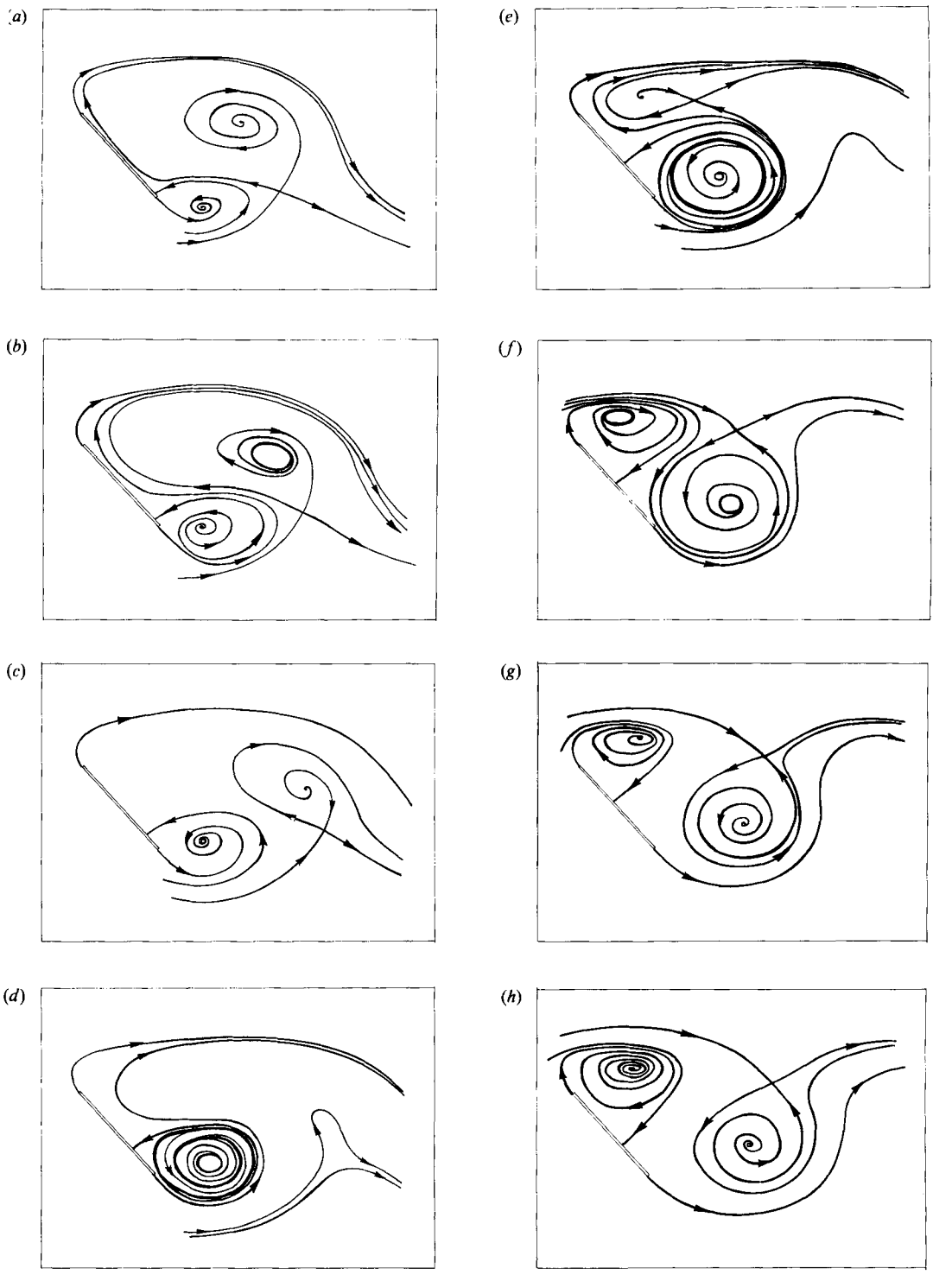

FIGURE 18(*a–h*). For caption see facing page.

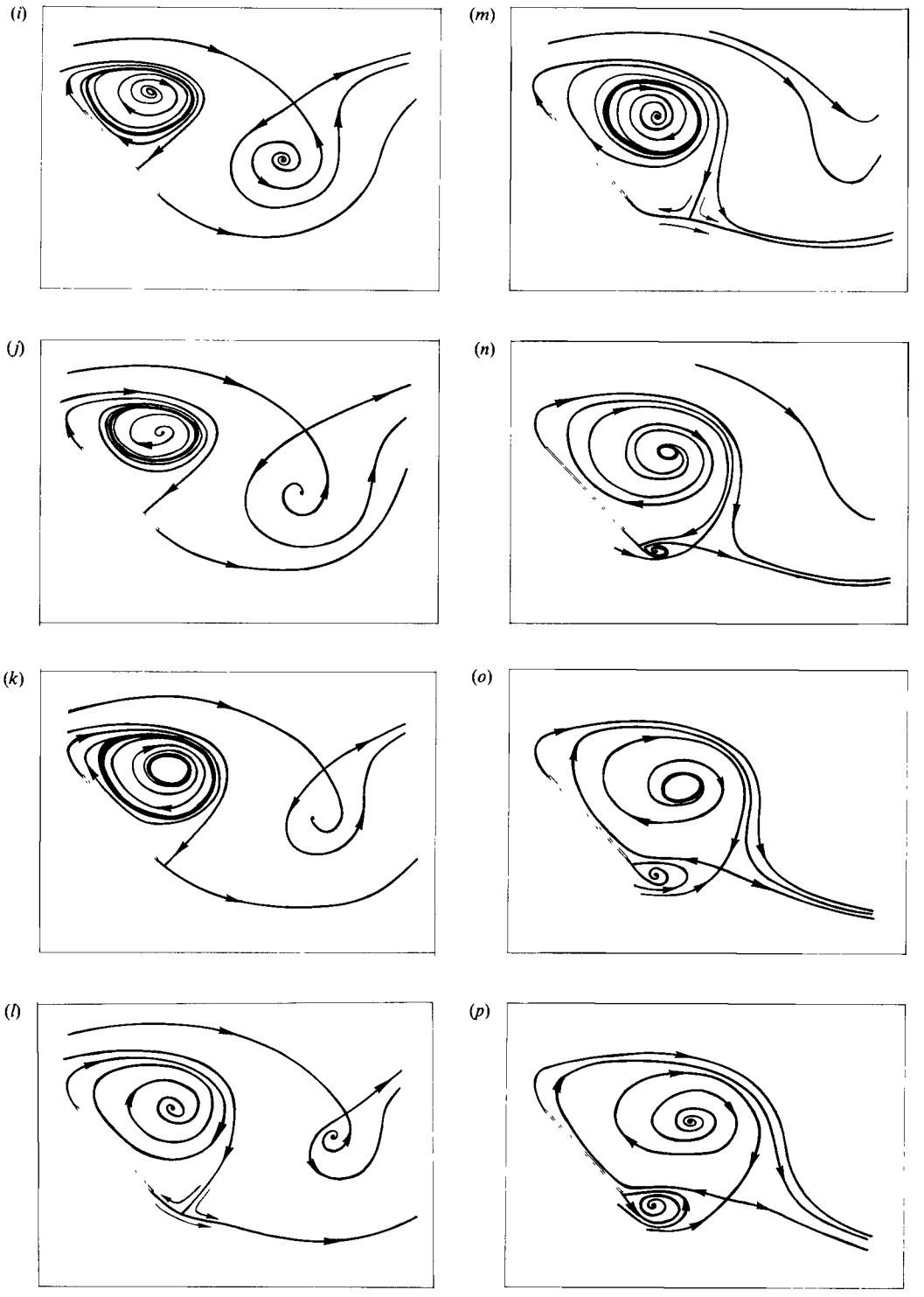

FIGURE 18. Interpretations of patterns shown in figure 17.

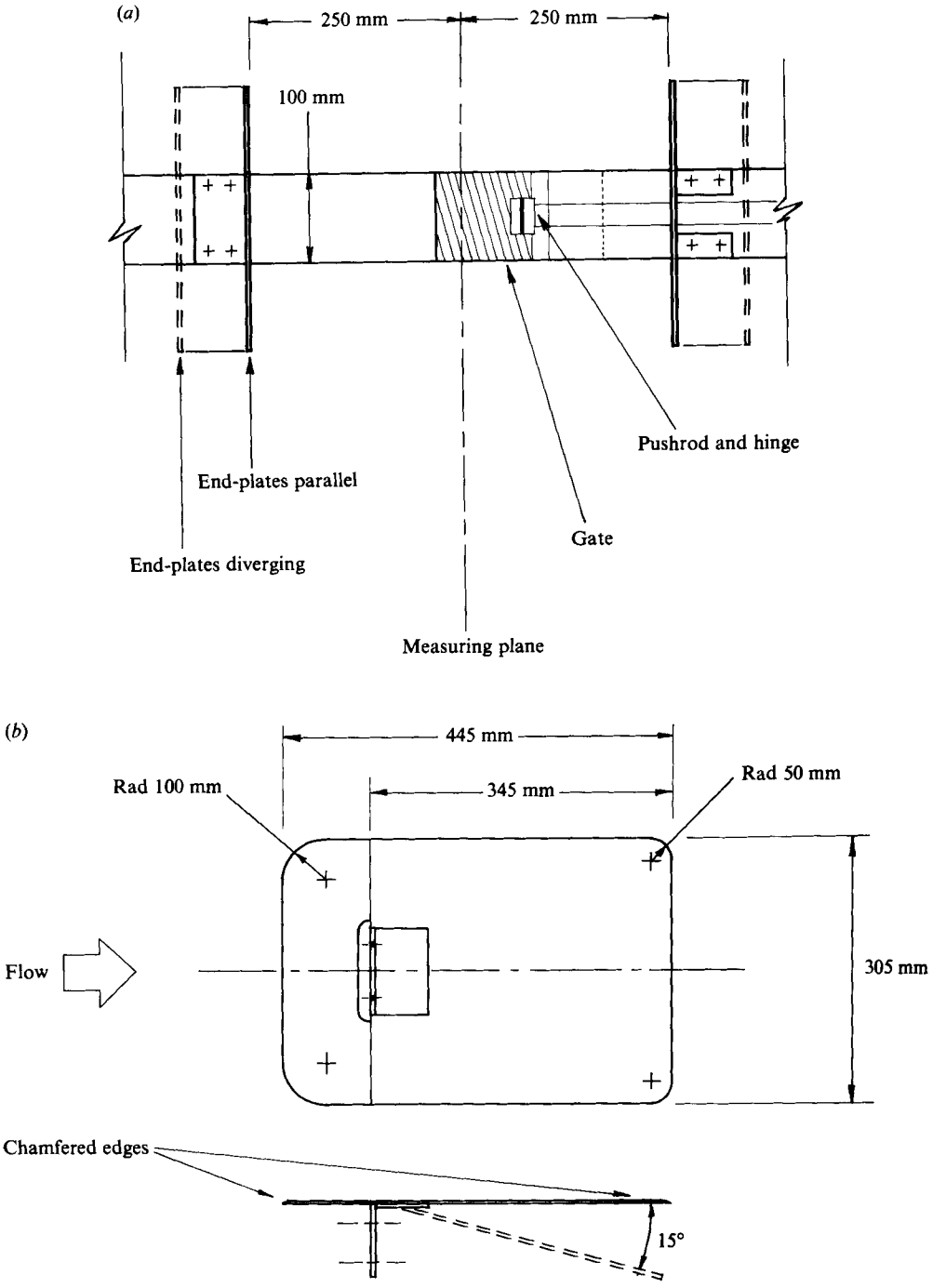

FIGURE 19. Design and attachment of end plates. Attachment of end plates (*a*) is as viewed from the rear of the body.

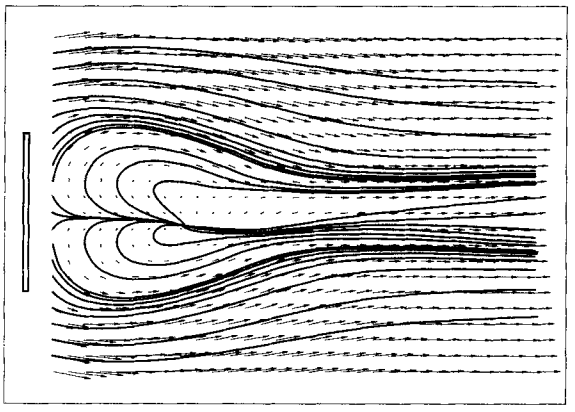

FIGURE 20. Mean velocity vector field and integrated streamline pattern for the case of a nominally two-dimensional bluff plate set normal to the free-stream flow, and with end plates set parallel to each other. The observer is at rest with respect to the bluff body.

reduction in effective aspect ratio A of the bluff body when end plates were attached: A is reduced from 9.4 to 5. It was nevertheless decided to gather data behind the bluff body with end plates both set parallel and diverging in order to determine the effect that varying the end conditions had on the near-wake flow patterns. The unexpectedly high degree of three-dimensionality for these cases was considered to be of interest since it graphically demonstrates how sensitive the cavity-region flow is to end conditions. In addition patterns with interesting topological properties are produced.

Figure 20 shows the temporal mean flow for the case with parallel end plates, and no eddying motions are apparent. The phase-averaged patterns for eight phases of the cycle are given in figure 21. Here as in the previous normal-plate case the vortex shedding was assumed to be antisymmetrical. The cavity vortices appear to be confined closer to the plate than when no end plates were fitted. Figure 22 shows interpretations of the different phases for this case.

The temporal mean pattern for the case with diverging end plates is shown in figure 23. Figures 24 and 25 give the phase-averaged patterns and their interpretations respectively. For this case the cavity appears to be completely detached from the plate at all phases, and vortex roll-up occurs further downstream than is evident in any of the preceding flows. This unexpected behaviour was verified using flow-visualization techniques. In this nominal plane of symmetry the plate appears to behave as if it were porous. In fact the plate would have a series of nodes and saddles located on it as given in figure 1 (r). Considering phase 1 in figure 25, the simplest pattern that is topologically equivalent is sketched in figure 26.

4. Convergence of data and the existence of limit cycles

In the Appendix, the convergence of data is examined and it is concluded that the various flow-pattern features discussed are real. False limit cycles can occur if the data has not converged but from the analysis given in the Appendix it appears that most of the limit cycles are real. A limit cycle is consistent with the existence of a multi-celled vortex structure. Sullivan (1959) analysed a solution to the Navier–Stokes equation that has a two-celled vortex structure, sketched in figure 27 (a). It can be

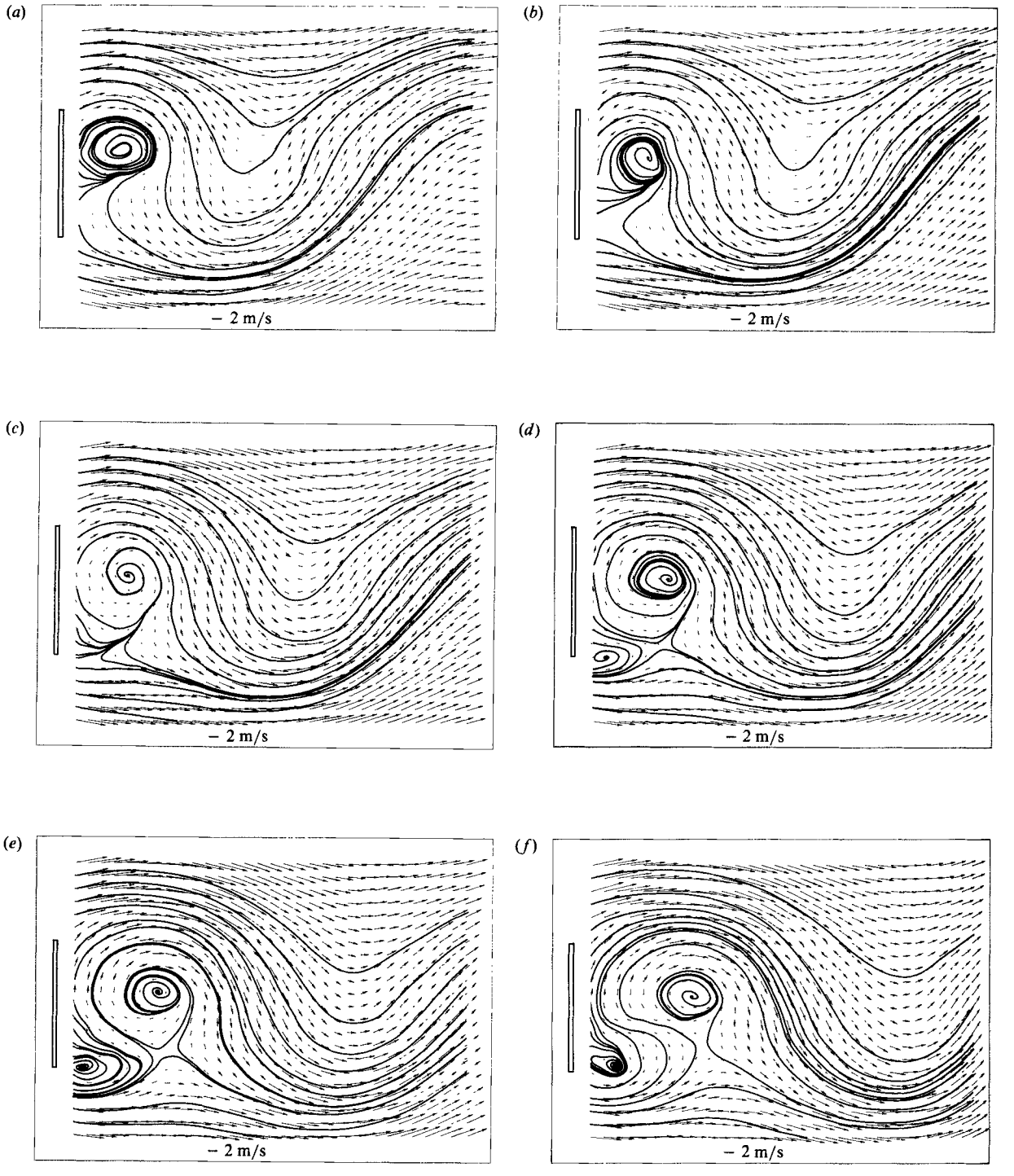

FIGURE 21 (*a–f*). For caption see facing page.

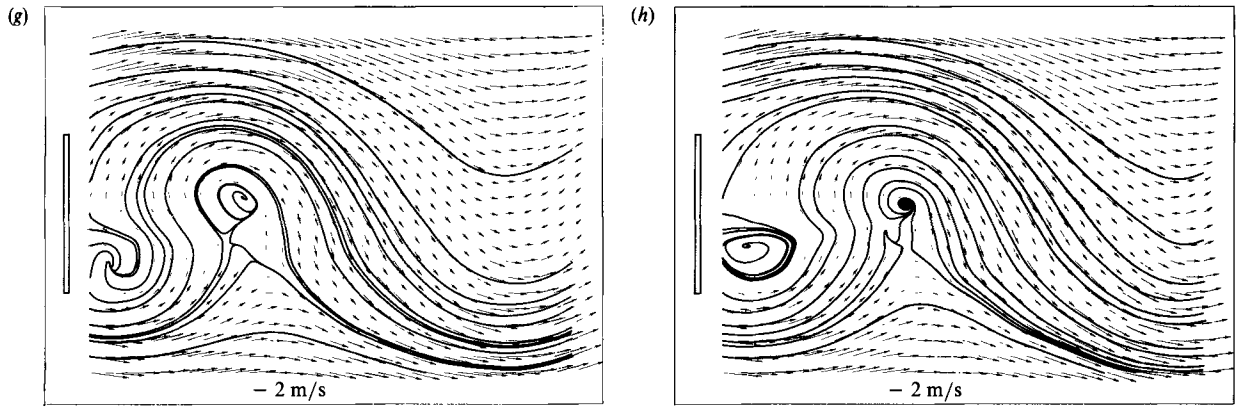

FIGURE 21. Velocity vector field and phase-averaged integrated streamline patterns behind normal bluff body with parallel end plates. (*a*)–(*h*) Respectively correspond to phases 1–8.

shown that the Sullivan vortex implies that vortex filaments are wound up into a peculiar 'bi-helical' form. A computed pictorial representation of such a vortex-filament configuration is shown in figure 27(*b*). The filaments are wound about cylindrical 'shells' into helices which have opposite-signed pitch angles on either side of the plane of symmetry. The helices are wrapped progressively tighter as one moves axially away from the plane of symmetry. This helical wrapping of the vortex filament may be associated with some possible spanwise waviness of the vortices shed from the body.

Whether this waviness is associated with a 'cellular' type of flow separation as observed by Korotkin (1976) and others from a circular cylinder is not known at this stage.

5. Discussion and conclusions

Phase-averaged vector fields and the associated streamline patterns are presented for flow in the nominal plane of symmetry of the near wake of some nominally two-dimensional bluff bodies. Patterns in the cavity region are produced using data obtained with reasonably high resolution for sixteen phases of the vortex-shedding cycle. Some turbulence quantities are also presented.

Of all the results presented here, the most useful information regarding the physical processes involved comes from the streamline patterns. Broadly speaking, the topological structure of the flow in the case of the normal bluff body without end plates is similar to that suggested by the two-dimensional laminar vortex-shedding patterns reported by Perry *et al.* (1982). There are however some important differences. The flow is obviously three-dimensional as evidenced by the appearance of foci and limit cycles. The precise nature of the three-dimensionality is not known at this stage but the authors suspect that a periodic waviness of the vortex cores in the spanwise direction is involved.

During parts of the shedding cycle the vortices are undergoing axial stretching and appear as stable foci in the plane of symmetry, and at other times axial compression leads to the appearance of unstable foci. The appearance of limit cycles seems to occur as part of the bifurcation process associated with such a change in the nature

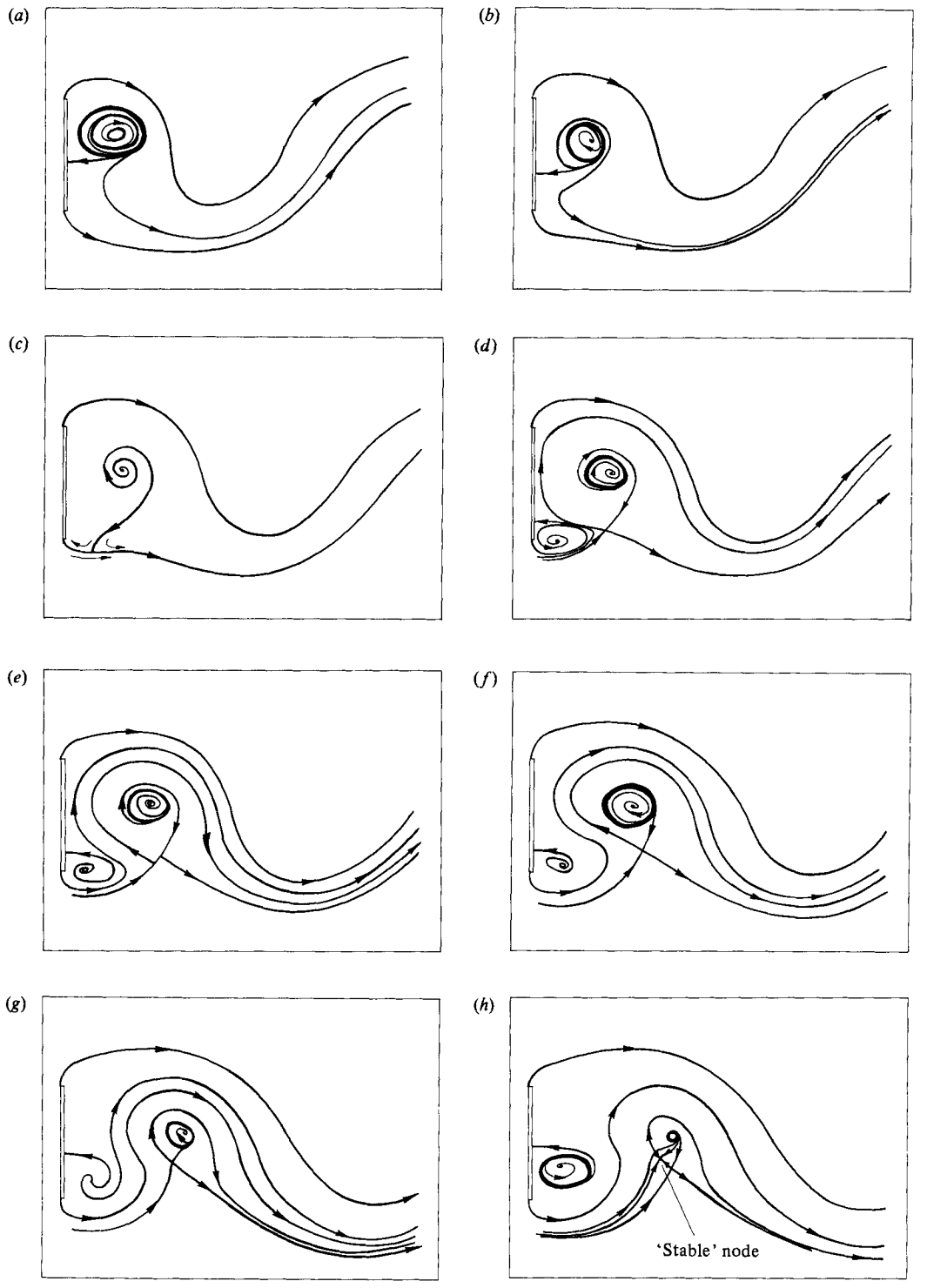

FIGURE 22. Interpretations of patterns shown in figure 21 (*a*)–(*h*) correspond respectively to phases 1–8.

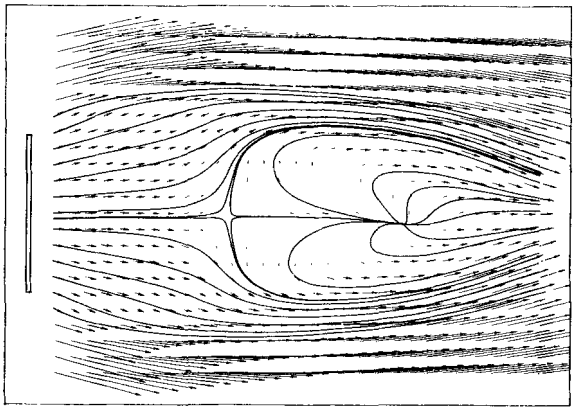

FIGURE 23. Mean velocity vector field and integrated streamline pattern for the case of a nominally two-dimensional bluff plate set normal to the free-stream flow, and with end plates diverging from each other. The observer is at rest with respect to the bluff body.

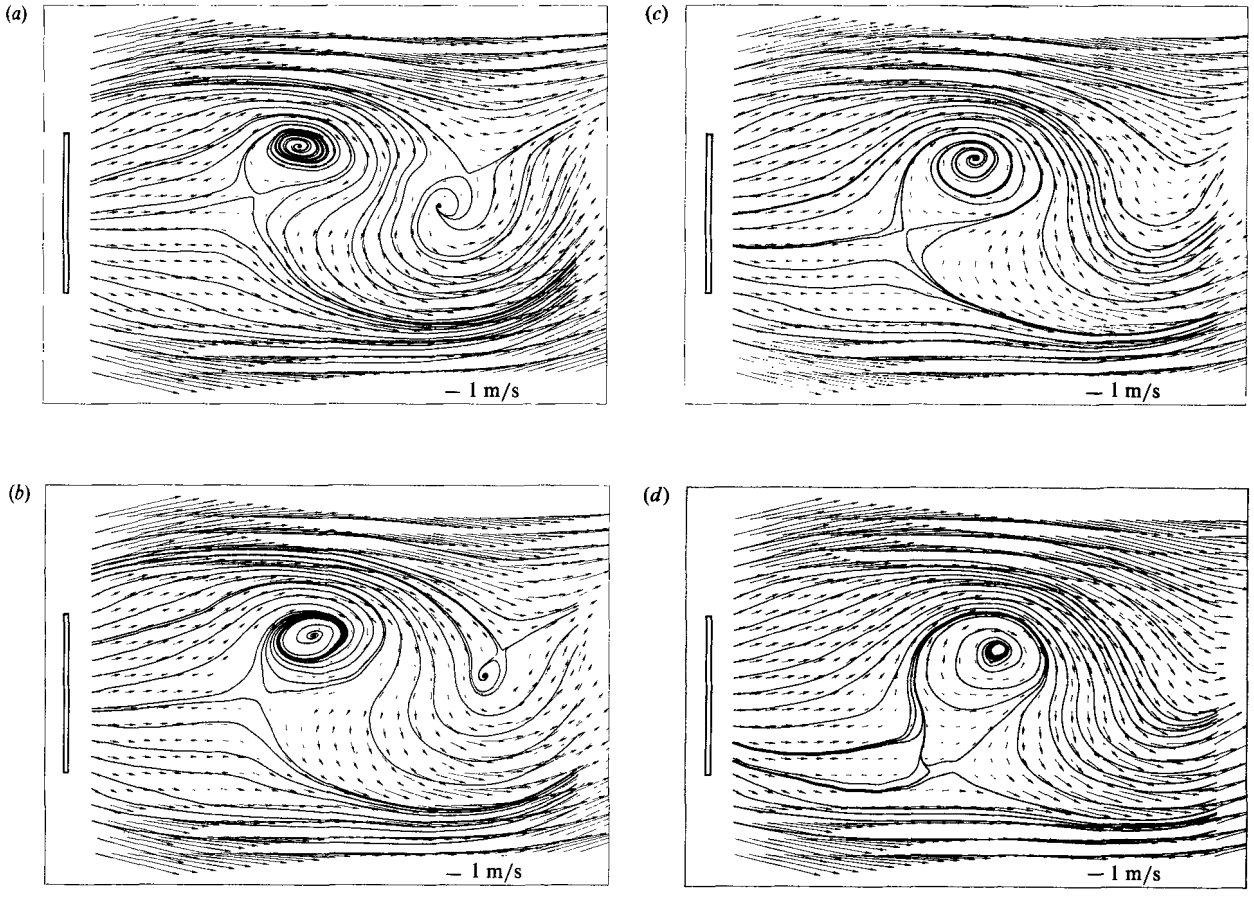

FIGURE 24 (*a–d*). For caption see next page.

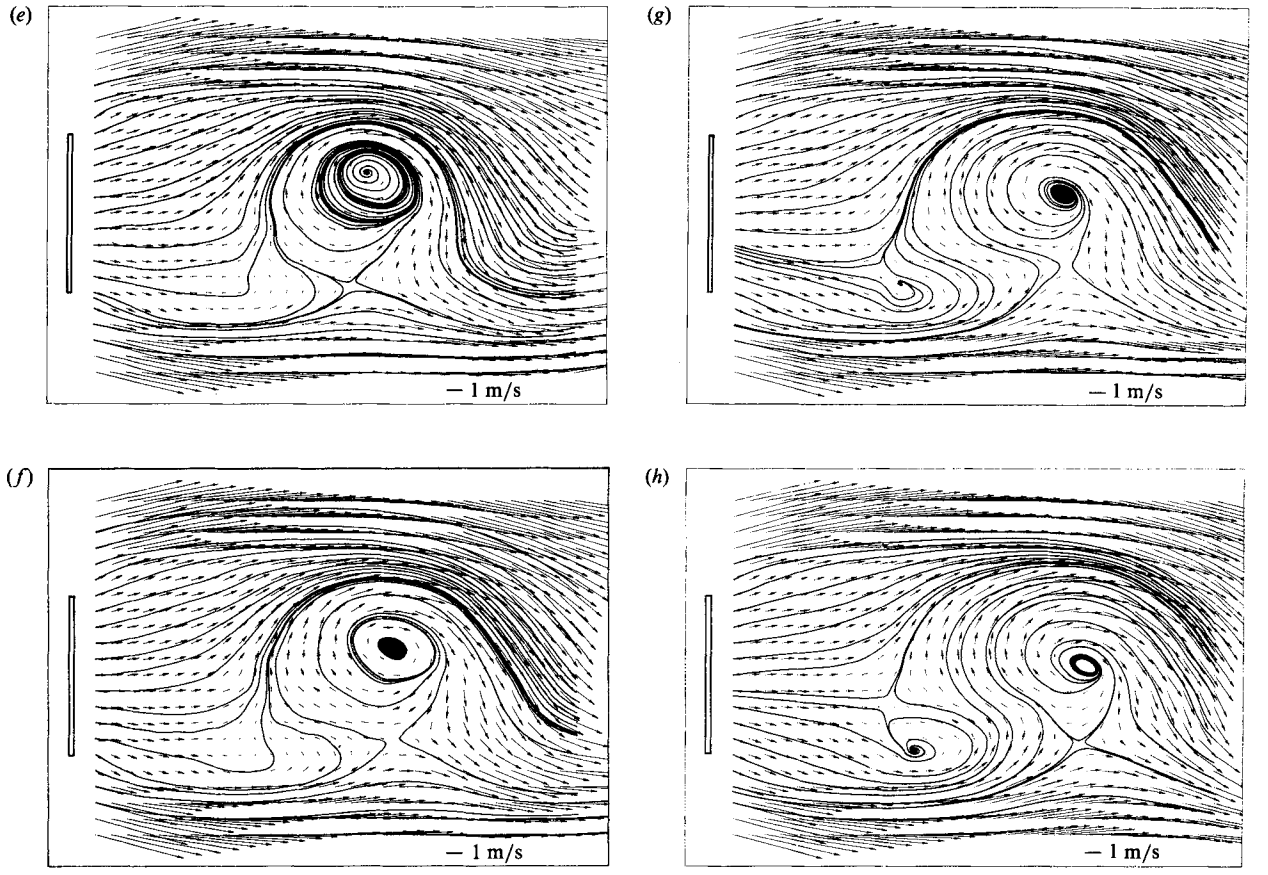

FIGURE 24. Velocity vector fields and phase-averaged streamline patterns behind normal bluff body with diverging end-plates. (*a*)–(*h*) Correspond respectively to phases 1–8.

of a focus. From a study of the simple Sullivan vortex, which appears to resemble the observed patterns, such limit cycles can be explained in terms of vortex filaments being deformed into helices in the roll-up process.

The cavity region behind the inclined bluff plate is topologically similar to that of the normal bluff plate at any phase of the cycle. The residence time in the cavity of the vortex formed at the leading edge is longer than for the vortex forming at the trailing edge. This gives a rather unexpected mean-flow pattern behind the inclined plate.

The mean-flow patterns of the bluff plates set normal to the free-stream flow are not perfectly symmetrical, nor do they contain closed cavities as is usually assumed in descriptions of near wakes. For the normal bluff plate with end plates, the results indicate that the flow patterns are highly sensitive to the end conditions. The mean flow patterns in the cavity region have undergone a dramatic change in topological structure. The phase-averaged vector fields indicate that the alignment of the end plates may have a strong influence on the position of the foci, and hence of the location of vortex roll-up. Parallel end plates caused vortex formation to occur close to the body, whereas diverging end plates led to vortex roll-up taking place further from the body.

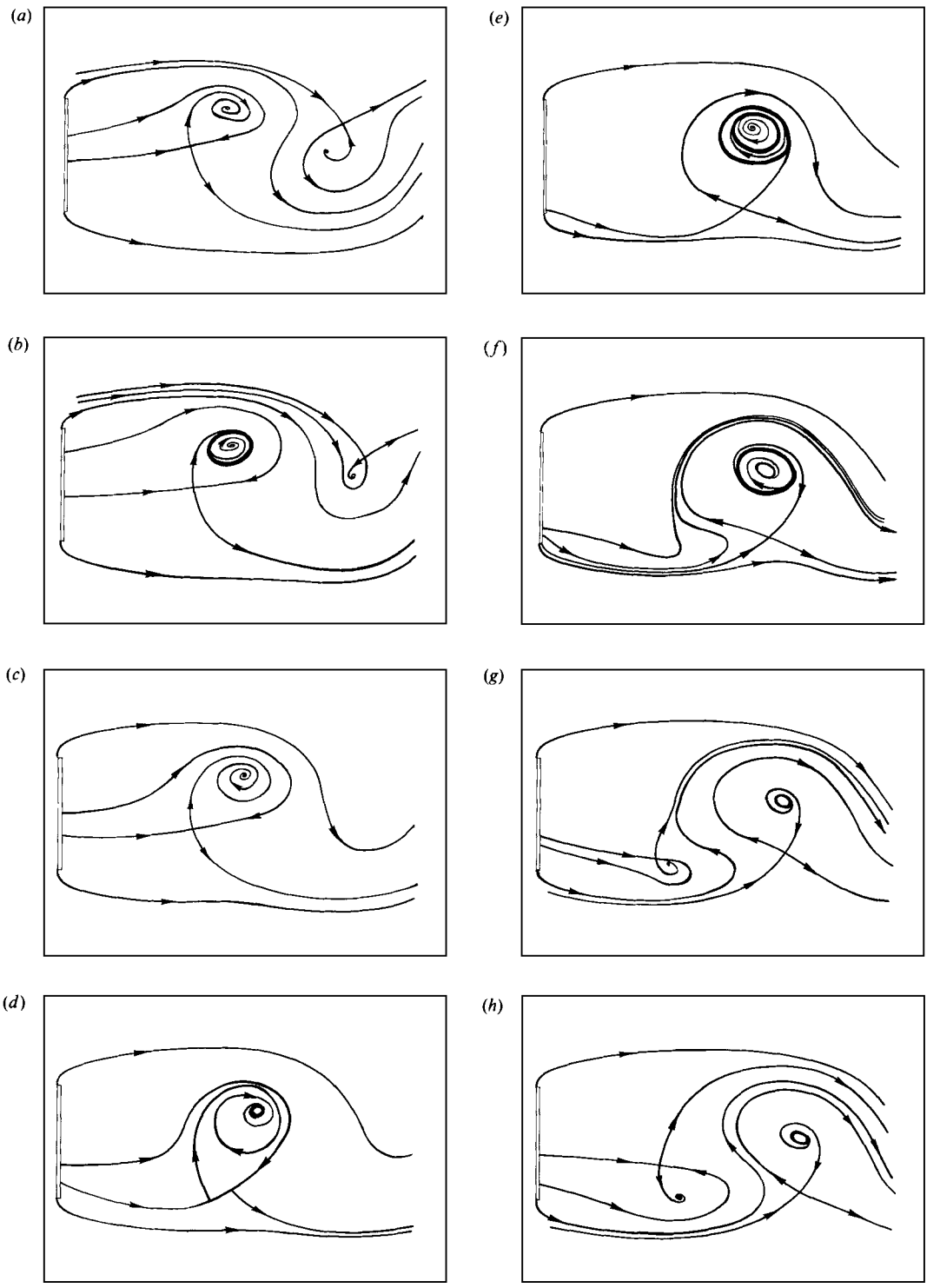

FIGURE 25. Interpretation of patterns shown in figure 24. (*a*)–(*h*) correspond respectively to phases 1–8.

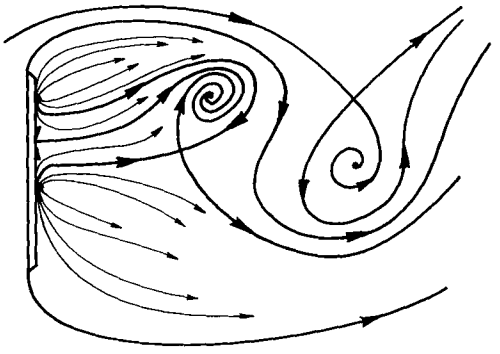

FIGURE 26. Simplest non-degenerate pattern that is topologically equivalent to phase 1 in figure 25.

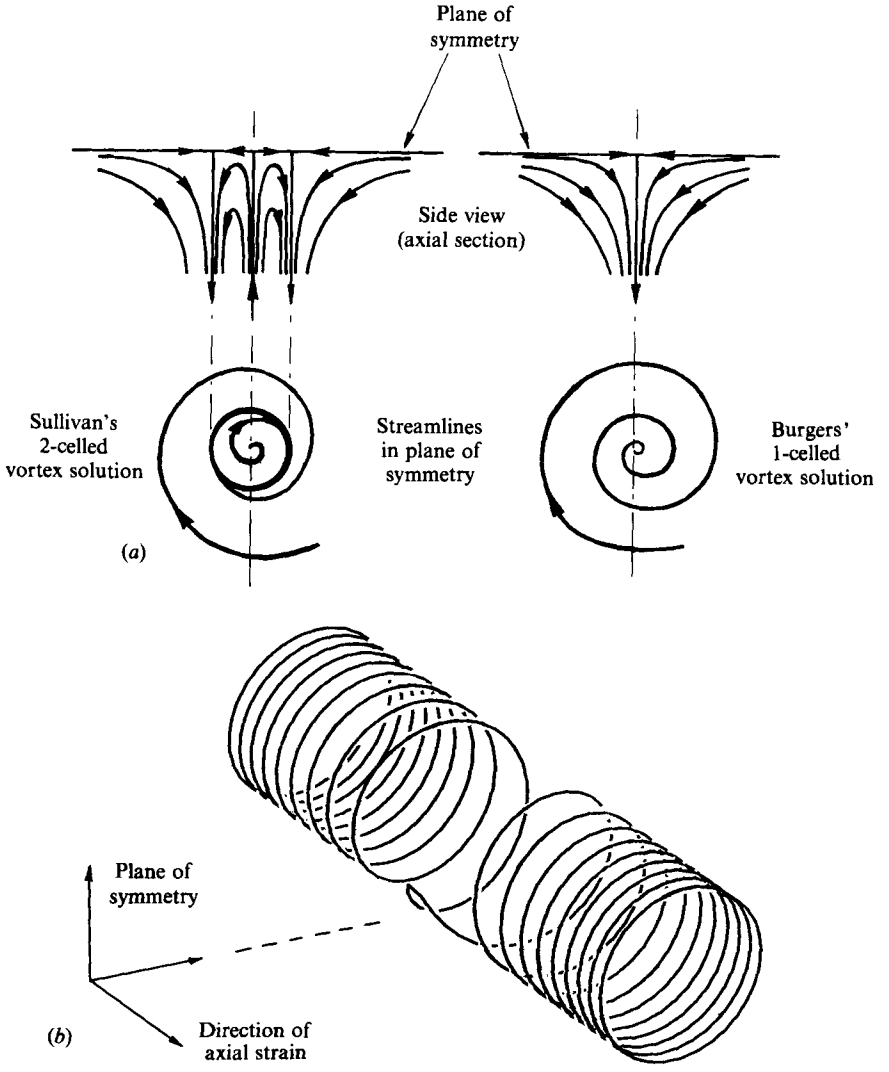

FIGURE 27. (*a*) A comparison of the structure of a two-celled Sullivan vortex with that of the single-called Burgers' vortex. (*b*) A computed view of a vortex filament in a Sullivan vortex.

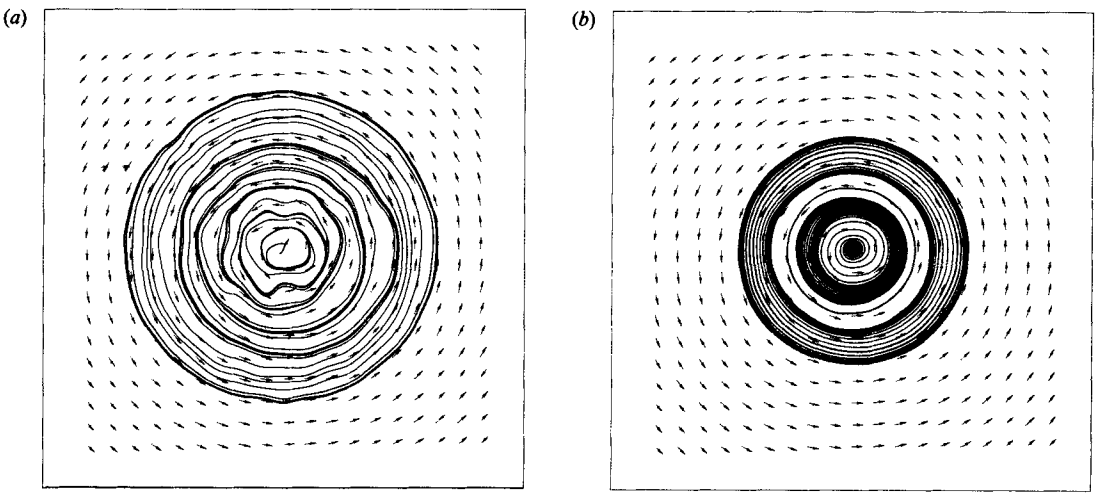

FIGURE 28. (*a*) Velocity vector field and integrated streamline pattern for solid body rotation with 3% degree of randomization (no smoothing applied). (*b*) Same as for (*a*), except that 3-point smoothing has been applied in both the vertical and horizontal directions.

In the rather complex phenomenon of vortex shedding, it is difficult to decide what quantities are the most relevant to measure for gaining insights into the physical processes involved. Three-dimensional phase-averaged vorticity fields would seem to be the most relevant and useful since these would show how sheets are rolled-up and how vortex cores are deformed in the spanwise direction. The velocity field would be contained in such measurements and could always be recovered by using the Biot–Savart law. Unfortunately at this stage of development such measurements are out of our reach. We believe that in the field of computational fluid dynamics, turbulence modelling should be directed towards phase-averaged motions. This is at least one stage better than modelling on the basis of the time-averaged equations of motion and introduces the simplest form of time dependence. The quantities most conveniently produced for comparison with experimental results would be phase-averaged velocity vector fields and phase-averaged streamline patterns. This work, like that of Cantwell & Coles, shows that time-averaged motions bear little resemblance to phase-averaged motions and any attempt to model such flows with global time-averaged equations appears to be far removed from reality. Unless computational methods can produce patterns similar to those experimentally observed in nature such as those presented here, such activities will always remain unconvincing.

Appendix A. Smoothing of data convergence and the existence of limit cycles

It is very difficult to objectively distinguish random variations in the data from genuine variations indicative of fluid-dynamical features. Excessive smoothing may remove some important features, while insufficient smoothing may leave the data too sensitive to the random variations. As a guide for deciding whether or not the smoothing used here was justifiable when the data had not fully converged, a known analytical solution was tested. The pattern generated for an idealized solid-body-rotation flow is a set of concentric circular streamlines. Figure 28(*a*) shows the

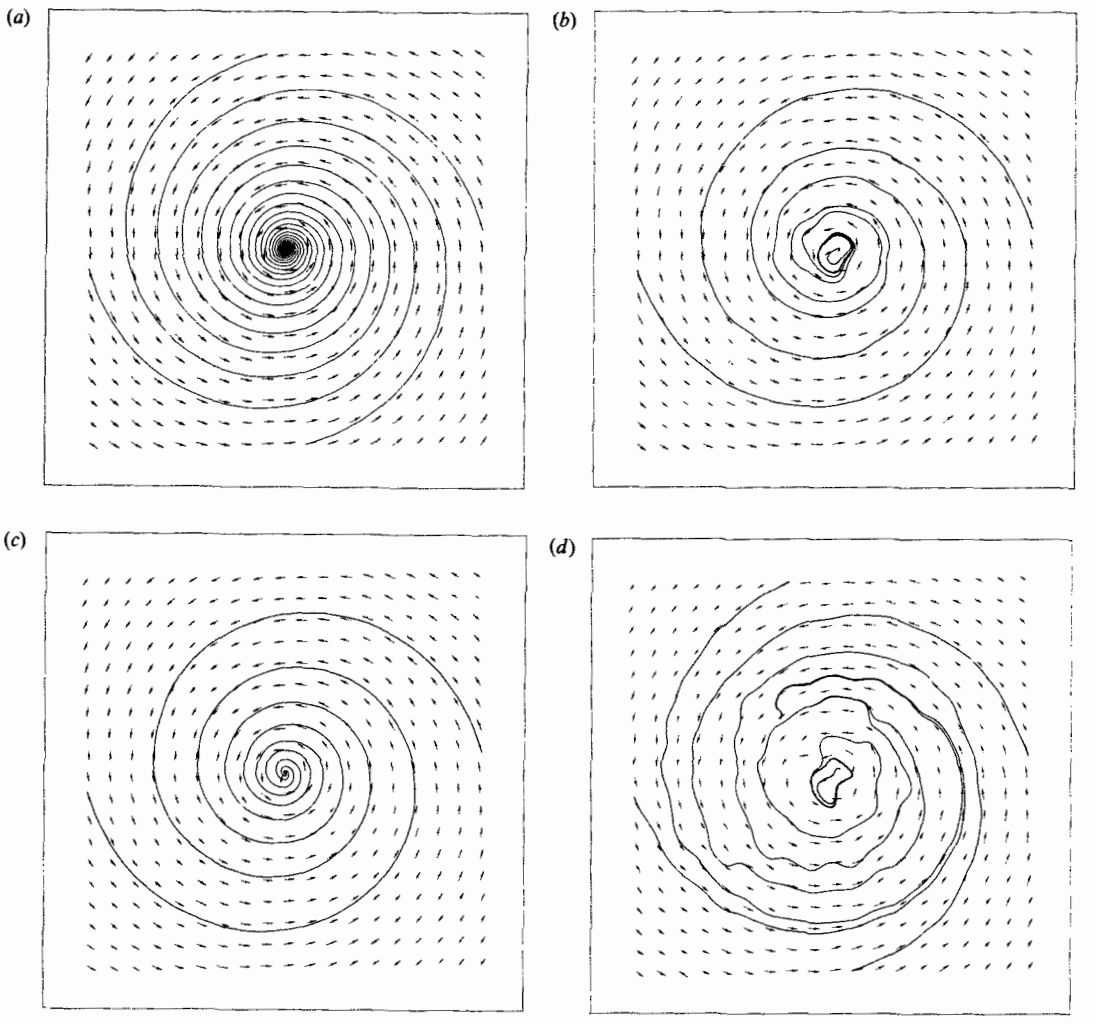

FIGURE 29(*a–d*). For caption see facing page.

velocity field and integrated streamline pattern one obtains when the velocity components have a random component added to them. This random component simulates a lack of convergence of the data and was generated with a Gaussian p.d.f. For the purposes of this work we shall use the term 'degree of randomization', say, in figure 28(*a*) as the ratio of the r.m.s. random component of velocity to the r.m.s. value of all velocity components shown in the corresponding 'perfectly converged' vector field.

Figure 28(*a*) shows that a 3 % degree of randomization has caused a change in the topological structure of the pattern from a centre to a set of nested limit cycles. A centre is a degenerate pattern and hence is structurally unstable so that any slight lack of convergence can lead to changes in the topological structure. The emergence of a set of nested limit cycles in this case suggests that if the flow is close to two-dimensional, i.e. the streamlines spiral into or out from foci at a slow rate, then the observed topological structure may be very sensitive to a lack of convergence of the data. The result of 3-point smoothing along and across the rows of data is shown

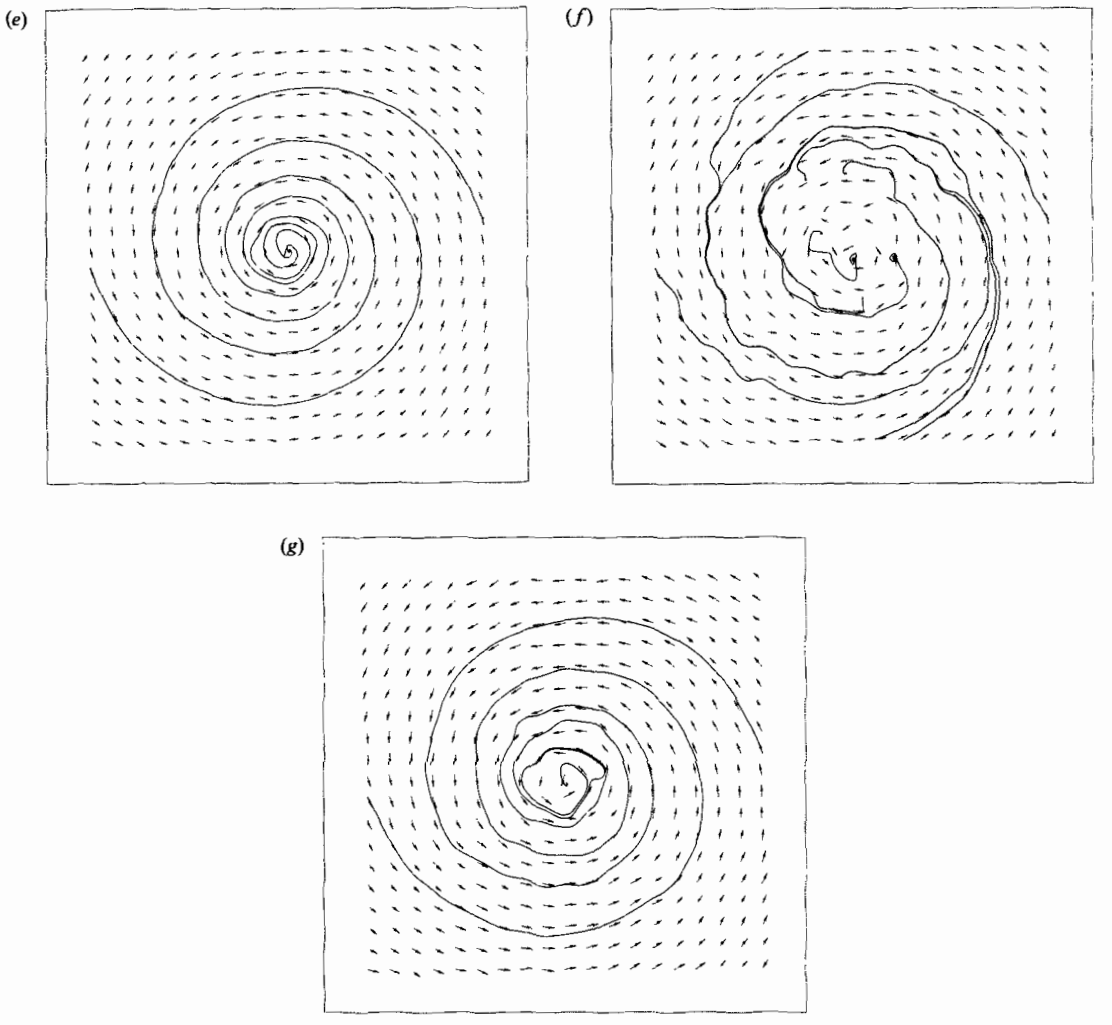

FIGURE 29. (*a*) Velocity vector field and integrated streamline pattern for a Burgers' vortex (plane of symmetry). (*b*) Same as (*a*), except that a 3% degree of randomization has been applied to the velocity components. (*c*) Same as (*b*), except that 3-point smoothing has been applied to the 'randomized' data. (*d*) Same as (*a*), except that a 9% degree of randomization has been applied to the Burgers' vortex velocity field. (*e*) Same as (*d*) except that multiple-point smoothing has been applied. (*f*) Same as (*a*), except that a 18% degree of randomization has been applied to the Burgers' vortex velocity field. (*g*) Same as (*f*), except that multiple-point smoothing has been applied.

in figure 28(*b*). This is identical with the second stage of smoothing applied to the experimental data as described in §2.3. It can be seen that the pattern still consists of nested limit cycles but that now the streamlines are less irregular.

The situation is different where foci have streamlines spiralling in or out at an appreciable rate. Figure 29 shows the effect of increasing the degree of randomization of the velocity components of a so-called Burgers' vortex (see Burgers 1948), and then applying 3-point smoothing. Figure 29(*a*) shows the idealized Burgers' vortex that models a viscous vortex undergoing axial strain. The solution is steady and satisfies the Navier–Stokes and continuity equations. With 3% randomization the

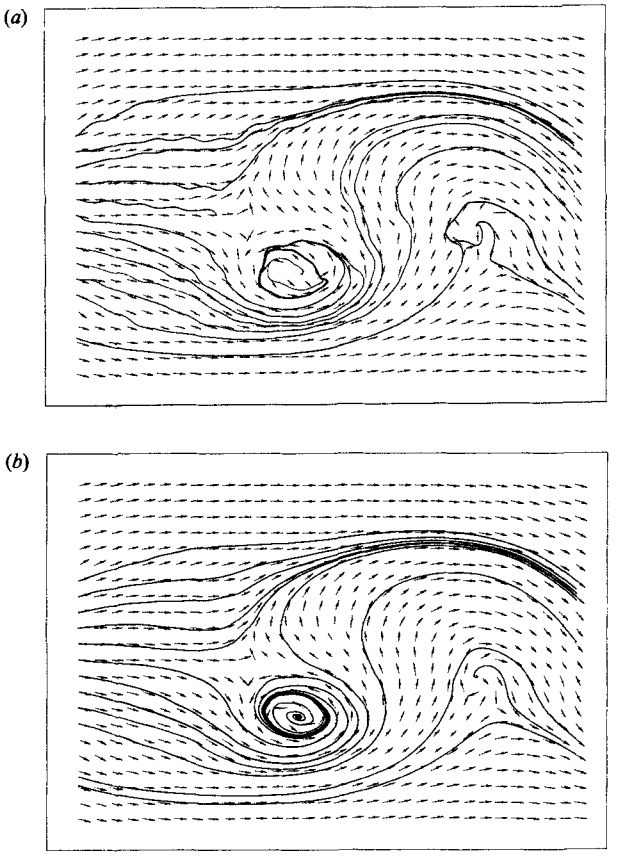

FIGURE 30. (*a*) Experimental data (phase 2 figure 24 (inverted)) before 3-point smoothing in the streamwise and cross-stream directions (but after smoothing along rows weighting data according to sample population). (*b*) Same as (*a*), except that multiple-point smoothing has been applied.

pattern is largely unchanged, except for a slight waviness in the streamlines and the appearance of a small limit cycle. This is shown in figure 29(*b*). Data yielding the pattern in figure 29(*b*) was then 3-point smoothed to produce the pattern in figure 29(*c*). This pattern has the same topological structure as the original 'perfectly converged' pattern. The appearance of the two patterns is very similar as streamlines spiral in at about the same rate.

Figures 29(*d*, *e*) show the effect of 9% randomization with and without smoothing respectively. The randomization of the velocity components leads to very wavy integrated streamlines in figure 29(*d*), and one node and a small limit cycle have appeared. After 3-point smoothing the topological structure of the underlying Burgers' vortex has re-emerged.

Increasing the degree of randomization to 18% and integrating to obtain figure 29(*f*) we have altered the topological structure. Many extraneous critical points have been generated by the 'lack of convergence', but although each one has only a localized effect, the original pattern appears disguised. No limit cycles are evident however. By simple 3-point smoothing of the data (see figure 29(*g*)) a pattern very similar in appearance, and topologically identical with, the original Burgers' vortex is revealed. Clearly, experimental data giving such a 'chaotic' pattern as that shown

in figure 29(*f*) would not be acceptable although it may be seen that simple 3-point smoothing can be surprisingly effective in extracting the underlying large-scale behaviour from a set of badly converged data.

We have seen that apparent limit cycles may be produced when the data are badly converged. However, without exception they were localized to one or two data grid elements regardless of the actual scale of the grid involved and they were removed by smoothing the data. The limit cycles observed in the experimental data behaved differently as they are not so severely localized, and are not removed by smoothing. This is shown in figure 30, where (*a*) shows experimental data prior to 3-point smoothing along and across the horizontal rows, and (*b*) the same data smoothed. This data belongs to one phase of the vortex-shedding cycle of the wake of a normal bluff body with end plates diverging (figure 24, phase 2). From the appearance of the pattern before the data is smoothed the degree of randomization, or lack of convergence, was estimated to be of the order of 3 %.

We may conclude from this work that small limit cycles that can be removed by smoothing are probably not genuine features of the flow, but rather may be produced by lack of convergence of the data. On the other hand, limit cycles that are large and remain substantially unaltered after smoothing should be treated as genuine features of the fluid dynamics involved.

Furthermore, in an experimental situation where only a finite sample population can be gathered, it is possible that a series of nested limit cycles is indicative of a region of nearly two-dimensional vortical flow. This behaviour is seen in the temporal mean-flow pattern in figure 6(*a*). Such a flow pattern should be treated with caution. However, the authors believe that many of the experimentally obtained limit cycles are real. Perry & Tan (1984) encountered limit cycles in their deterministic experiments with co-flowing jets and wakes even though their technique of producing integrated streamlines differs from the method used here.

REFERENCES

BURGERS, J. M. 1948 A mathematical model illustrating the theory of turbulence. *Adv. Appl. Mech.* **1**, 171–199.

CANTWELL, B. J. 1976 A flying hot-wire study of the turbulent near wake of a circular cylinder at a Reynolds number of 140000. Ph.D. thesis, California Institute of Technology.

CANTWELL, B. J. & COLES, D. 1983 An experimental study of entrainment and transport in the turbulent near wake of a circular cylinder. *J. Fluid Mech.* **136**, 321–374.

DAVIES, M. E. 1976 A comparison of the wake structure of a stationary and oscillating bluff body, using a conditional averaging technique. *J. Fluid Mech.* **75**, 209–231.

GRAHAM, J. M. R. 1969 The effect of end-plates on the two-dimensionality of a vortex wake. *Aero. Quart.* August 1969, pp. 237–247.

HORNUNG, H. G. & PERRY, A. E. 1984 Some aspects of three-dimensional separation, part 1: streamsurface bifurcations. *Z. Flugwiss. Weltraumforschung* **8**, 77–87.

KAPLAN, W. 1958 *Ordinary Differential Equations.* Addison-Wesley and Pergamon.

KOROTKIN, A. I. 1976 The three dimensionality of the flow transverse to a circular cylinder fluid mechanics. *Sov. Res.* **5**, 96–103.

LIGHTHILL, M. J. 1963 In *Laminar Boundary Layers* (ed. L. Rosenhead), pp. 48–88. Oxford University Press.

MINORSKY, N. 1947 *Non-Linear Mechanics.* J. W. Edwards.

MINORSKY, N. 1962 *Non-Linear Oscillations.* Van Nostrand.

NIELSEN, K. W. 1970 Vortex formation in a two-dimensional periodic wake. Ph.D. thesis, Oxford University.

OSWATITSCH, K. 1957 Die Ablongsungsbedingung von Grenzshichten. In *Grenzschicht Forschung* (ed. H. Goertler), p. 357. Springer.

PERRY, A. E. 1982 *Hot-Wire Anemometry*. Clarendon.

PERRY, A. E. 1984*a* A study of degenerate and non-degenerate critical points in three-dimensional flow fields. *DFVLR Forschungsbericht FB* 84-36.

PERRY, A. E. 1984*b* A series expansion study of the Navier–Stokes equations. *DFVLR Forschungsbericht FB* 84-34.

PERRY, A. E., CHONG, M. S. & LIM, T. T. 1982 The vortex shedding process behind two-dimensional bluff bodies. *J. Fluid Mech.* **116**, 77–90.

PERRY, A. E. & FAIRLIE, B. 1974 Critical points in flow patterns. *Adv. Geophys.* B**14**, 299–315.

PERRY, A. E. & HORNUNG, H. G. 1984 Some aspects of three-dimensional separation, part 2: vortex skeletons. *Z. Flugwiss. Weltraumforschung* **8**, 155–160.

PERRY, A. E. & LIM, T. T. 1978 Coherent structures in coflowing jets and wakes. *J. Fluid Mech.* **88**, 451–463.

PERRY, A. E., LIM, T. T. & CHONG, M. S. 1980 The instantaneous velocity fields of coherent structures in coflowing jets and wakes. *J. Fluid Mech.* **101**, 243–256.

PERRY, A. E. & TAN, D. K. M. 1984 Simple three-dimensional vortex motions in coflowing jets and wakes. *J. Fluid Mech.* **141**, 197–231.

PERRY, A. E. & WATMUFF, J. H. 1981 The phase-averaged large-scale structures in three-dimensional turbulent wakes. *J. Fluid Mech.* **103**, 33–51.

ROSHKO, A. 1954 On the drag and shedding frequency of two-dimensional bluff bodies. *NACA Tech. Note* 3169, July 1954.

STEINER, T. R. 1984 The study of turbulent wakes and the vortex shedding process. Ph.D. thesis, University of Melbourne.

STEINER, T. R. & PERRY, A. E. 1986 Large-scale vortex structures in turbulent wakes behind bluff bodies. Part 2. Far-wake structures. *J. Fluid Mech.* **174**, 271–298.

SULLIVAN, R. D. 1959 A two-celled solution of the Navier–Stokes equations. *J. Aero. Sci.* **26**, 767–768.

WATMUFF, J. H., PERRY, A. E. & CHONG, M. S. 1983 A flying hot-wire system. *Exps in Fluids* **1**, 63–71.